Heterogeneous Graph Neural Network for Power Allocation in Multicarrier-Division Duplex Cell-Free Massive MIMO Systems

Bohan Li, Lie-Liang Yang, *Fellow, IEEE*, Robert G. Maunder, *Senior Member, IEEE*, Songlin Sun, *Senior Member, IEEE*, Pei Xiao, *Senior Member, IEEE*

***Abstract*—In order to maximize the spectral efficiency (SE) in multicarrier-division duplex (MDD) enabled cell-free massive MIMO (CF-mMIMO), a heterogeneous graph neural network (HGNN), referred to as CF-HGNN, is specifically introduced to optimize the power allocation (PA). To efficiently manage the interference invoked, a meta-path based mechanism is applied in CF-HGNN to enable individual access point (AP) and mobile station (MS) nodes to aggregate information from the interfering and communication paths with different priorities during message passing. Moreover, the proposed CF-HGNN employs the adaptive node embedding layer and adaptive output layer to make it scalable to the various numbers of APs, MSs and subcarriers. For comparison, a quadratic transform and successive convex approximation (QT-SCA) algorithm is proposed to solve the PA problem in classic way. Numerical results show that CF-HGNN is capable of achieving 99% of the SE achievable by QT-SCA but using only 10^{-4} times of its operation time, and it can outperform the conventional learning-based and greedy unfair methods in terms of SE performance. Furthermore, CF-HGNN exhibits good scalability to the CF networks with various numbers of nodes and subcarriers, and also to the large-scale CF networks when assisted by user-centric clustering.**

***Index Terms*—Multicarrier-division duplex, cell-free massive MIMO, heterogeneous graph neural network, power allocation.**

I. Introduction

With the unprecedented increase of data-hungry devices, wireless communication communities have been continuing to thrive in the last few years to seek the cutting-edge techniques for further improving spectral efficiency (SE) and quality of services (QoSs). In this regard, cell-free massive MIMO (CF-mMIMO) and in-band full-duplex (IBFD) have been envisioned as the main pillars of future wireless communication systems [1, 2]. However, to date, although there exist a large number of works on CF-mMIMO and IBFD, the combination of these two techniques has rarely been addressed. One of the underlying reasons is that, apart from the inherent self-interference (SI), IBFD-based CF (IBFD-CF) systems suffer from severe cross-link interference (CLI), also known as inter-AP interference (IAI) or inter-MS interference (IMI).

Specifically, the IBFD-CF was studied in [3] in the context of the centralized CF-mMIMO systems, where 'centralized' means that channel estimation, beamforming, SI/CLI cancellation and data detection are all done at a central processing unit (CPU). To manage CLI, authors resorted to the coordinated precoding and successive interference cancellation, but only a small amount of CLI can be mitigated, leading to that each AP/MS has to reduce its transmit power to decrease the CLI on the neighboring APs/MSs, and hence resulting in performance degradation. However, the CLI problem is much more intractable in the distributed IBFD-CF systems (where 'distributed' denotes that all signal processing tasks except data detection are performed at APs [1]), as the CPU without the access to global channel state information (CSI) is unable to implement the centralized CLI cancellation. Due to this, to the best of our knowledge, there is no published research works having considered the FD-style distributed CF-mMIMO systems. To fill the research gap, in [4], we proposed a distributed CF-mMIMO system driven by multicarrier-division duplex (MDD), which enables full-duplex (FD) operation in the same time slot and the same frequency band but on different subcarriers. In the MDD-assisted CF (MDD-CF) system, the subcarriers of one band are divided into two mutually exclusive subsets, namely downlink (DL) and uplink (UL) subcarrier subsets, to support DL and UL transmissions, respectively. With these arrangements, the SI/CLI and desired signals in MDD-CF are transmitted on the orthogonal subcarriers, and hence MDD-CF can be nearly free from the digital-domain SI and CLI by leveraging the fast Fourier transform (FFT) operated at the receivers of APs/MSs [5]. Our studies in [4] demonstrated that MDD-CF can significantly enhance system performance, when compared with IBFD-CF and TDD-CF.

However, in MDD-based systems, DL and UL transmissions are strongly coupled and have to be optimized at the same time. On the other hand, CF-mMIMO consists of a huge number of AP/MS nodes and subcarriers. Consequently, the power allocation (PA) for rate maximization in MDD-CF is non-convex and computationally challeng-

B. Li, L.-L. Yang and R. Maunder are with the School of ECS, Univ. of Southampton, SO17 1BJ, UK. (E-mail: bl2n18, lly, rm@ecs.soton.ac.uk, https://www.ecs.soton.ac.uk/people/llyang). S. Sun is with the School of ICE, BUPT, China. P. Xiao is with the ICS, Home for 5GIC & 6GIC, University of Surrey, Guildford, Surrey, GU2 7XH, UK. (Email: p.xiao@surrey.ac.uk). This work was supported by the Engineering and Physical Sciences Research Council (EPSRC) Project under Grant EP/X01228X/1.

ing. To date, various optimization algorithms have been proposed for PA, including Dinkelbach's transform [3], alternating direction method of multipliers (ADMM) [6], dual decomposition [7] and successive convex approximation (SCA) [8]. While these approaches can in general converge to the local optimum within several iterations, their computational complexity grows exponentially with the increase of network size. Moreover, once there are network changes, these algorithms have to rerun for obtaining the updated solutions, which introduces extra computational cost and latency. As the result, these traditional methods can hardly be operated in a timely manner for the PA in multicarrier CF-mMIMO systems. Needless to say, the situation is more complicated in the FD-style scenarios. Accordingly, all the above-mentioned problems motivate us to design a more advanced learning-based PA strategy to enable high efficiency and scalability for operation in the distributed MDD-CF systems.

A. Related Works

Compared with the conventional methods, machine learning (ML) has shown its potential for solving the PA problem in wireless communications. For instance, in [9], a convolutional neural network (CNN)-based PA algorithm was proposed and shown to be superior to the conventional weighted minimum mean square error (WMMSE) method in terms of the achievable SE and computation time. In [10], the deep reinforcement learning (DRL)-based PA was leveraged to solve respectively the max-min and SE maximization problems in CF-mMIMO. In [11], the authors resorted to the deep CNN for maximizing SE in the CF-mMIMO, and demonstrated that the learning-based method can outperform the well-known use-and-then-forget-based PA method. In [12], a clustered deep neural network (DNN) model exploiting the large-scale fading information was introduced to implement PA in CF-mMIMO, showing that its performance is comparable to that of the WMMSE-assisted alternating direction method.

The aforementioned learning-based PA methods have been demonstrated to prevail over the traditional methods in terms of performance and complexity. However, none of them have considered to exploit the structures of wireless networks in the optimization process. Hence, they cannot be generalized to the unseen scenarios, such as the networks with varying sizes. To this end, the graph neural network (GNN) reaping the advantages of scalability, generalization and parallel execution has attracted significant research interests in wireless communications. Specifically, in [13], a wireless channel graph convolution network (WCGCN) was proposed for solving the PA and beamforming problem in device-to-device (D2D) communication systems. It was shown that the WCGCN trained on the basis of small-sized systems can be generalized to use for optimization in the large systems with higher density of devices and larger cell size. Additionally, the authors in [14] and [15] studied the GNN-assisted PA in ad hoc networks and the proposed methods significantly outperform the conventional methods owing to the GNN's generalizability. Nevertheless, the above-mentioned GNN models for ad hoc or D2D networks are all homogeneous, where only one type of nodes, e.g., transmitter-receiver pairs, exist and they carry the homogeneous contents as node features. Hence, these GNN models cannot be directly utilized in the heterogeneous networks consisting of various types of base stations (BSs), APs and MSs, which have distinctive node features in terms of transmit power constraint, beamforming vector, duplexing mode, and so on.

In order to make GNN applicable to heterogeneous graphs, heterogeneous Graph Neural Network (HGNN) was first proposed in [16] for graph mining tasks (e.g., link prediction and recommendation), and recently introduced to deal with the optimization problems in wireless communications field. Different from [13], the authors of [17] proposed an HGNN-based model to deal with a heterogeneous D2D system, where the transmitter-receiver pairs differ from each other in terms of the number of antennas at transmitter. An HGNN model was also proposed in [18] for the intelligent reflecting surface (IRS)-assisted multi-user multiple-input single-output (MU-MISO) systems. Correspondingly, a single IRS and multiple DL MSs form a naive heterogeneous graph, which is used to learn precoders and the reflective coefficients of the IRS. However, the authors only considered the scalability with respect to MSs, while the cases of multiple reflecting elements are neglected. In [19], an HGNN model, referred to as the bipartite graph neural network (BGNN), was introduced to design precoders for MU-MISO systems, where MSs and BS antennas are deemed as two types of nodes. Although the authors demonstrated the adaptability of the BGNN to CF networks, it can hardly handle the interference among the BSs in multi-cell heterogeneous networks or among the APs in CF-mMIMO, when each BS/AP only serves a part of MSs. Furthermore, in [20], an HGNN-based model was applied for PA in the multi-cell heterogeneous networks, where BSs and MSs are classified into two types of nodes, showing that HGNN is capable of outperforming the conventional GNN. However, as only BSs have node features and the specific node features are not considered at MSs, the proposed model is incompetent for the FD-based networks, where DL MSs and UL MSs coexist and also have distinct QoS requirements.

B. Motivations

Despite the great breakthrough made by the existing HGNN-related work, none of them can be applied to our MDD-CF systems, mainly owing to the following obvious reasons: (i) In CF-mMIMO, each AP equipped with multiple antennas can concurrently transmit signals to multiple MSs. On the other side, each MS is typically served by a cluster of APs. Consequently, the node features of APs and MSs may vary with the sizes of CF-mMIMO networks. (ii) The MDD-CF operated in FD mode has

two types of nodes, i.e., APs and MSs, and four types of edges, namely DL, UL, CLI and SI links. Therefore, each AP (MS) node can be connected with the neighboring MS (AP) nodes via the DL (UL) communication paths, and with the neighboring AP (MS) nodes via interference paths. Moreover, the information collected from neighboring nodes via different paths may have distinct impact on the message aggregation at the central node. Consequently, an MDD-CF network is depicted as an extremely complicated heterogeneous graph, for which the off-the-shelf HGNN models proposed for the cell-based networks operated in HD mode cannot be directly applied. Hence, to meet the challenges, in this paper, we propose a promising CF-HGNN model specifically designed for solving the PA problem in the distributed MDD-CF systems. To the best of our knowledge, this is the first HGNN-based network proposed for the FD-style wireless systems.

C. Contributions

The major contributions are summarized as follows:

- The PA problem for maximizing SE in the distributed MDD-CF systems is formulated under the constraint of QoS requirements, where the effect of residual SI and CLI are practically modeled. As MDD-CF is a multicarrier-based scheme and works in FD mode, the formulated problem has to consider the PA among DL and UL subcarriers at the same time, resulting in a multiple-ratio concave-convex fractional programming (MRCCFP) problem. In this regard, we take the advantages of the quadratic transform and successive convex approximation (QT-SCA) to develop an iterative algorithm, which allows to converge quickly to the optimal solution. Furthermore, the feasible initialization, convergence behavior and computational complexity of the QT-SCA algorithm are analyzed. It is noteworthy that, since no study to date has investigated the PA problem in the FD-style multicarrier CF-mMIMO, the QT-SCA algorithm can be used as the prime benchmark to demonstrate the performance of the proposed HGNN-based method.
- To achieve the scalability and make the optimization general, we further propose the CF-HGNN to solve the formulated PA problem from ML perspective. In our CF-HGNN, an adaptive node embedding layer and an adaptive output layer are implemented so that the CF-HGNN can adapt to the MDD-CF networks with various numbers of APs, MSs and subcarriers. Two types of meta-paths are defined, namely the data transmission path and interfering path, to connect the involved AP/MS nodes. Furthermore, to learn the importance factors of the information received at the AP/MS nodes via two meta-paths during message passing, the meta-path attention mechanism is implemented with the CF-HGNN.
- We conduct a range of experiments to evaluate the effectiveness of the CF-HGNN for solving the PA problem in the distributed MDD-CF systems. Simulation results show that, without exploiting any prior information, the CF-HGNN is capable of learning nearly the same PA strategy as the QT-SCA algorithm, and outperforming the conventional learning-based and greedy unfair methods in terms of SE performance. Our studies also demonstrate that the CF-HGNN has the advantages over the QT-SCA in terms of computational complexity and operation time. Furthermore, the CF-HGNN exhibits the scalability to the MDD-CF networks with various numbers of nodes and subcarriers. Specifically, assisted by user-centric clustering, the CF-HGNN exhibits the scalability to the large-scale MDD-CF networks, which cover large area and simultaneously support a big number of nodes.

II. System Model

An MDD-CF system as shown in Fig. 1 is considered. Denote the set $\mathcal{D} = \{1, ..., d, ..., D\}$ for the single-antenna MSs and the set $\mathcal{L} = \{1, ..., l, ..., L\}$ for the APs of each with N antennas. Both APs and MSs are operated in the MDD mode relying on the mutually orthogonal subcarrier sets in the same band [21]. The DL subcarrier set is $\mathcal{M} = \{1, ..., m, ..., M\}$ with $|\mathcal{M}| = M$ and the UL subcarrier set is $\bar{\mathcal{M}} = \{1, ..., \bar{m}, ..., \bar{M}\}$ with $|\bar{\mathcal{M}}| = \bar{M}$. The total number of subcarriers is $M_{\text{sum}} = M + \bar{M}$. In particular, each AP can simultaneously serve all the MSs using any subcarrier in $\mathcal{M}$, while at the same time, each MS is able to send UL data over any subcarrier in $\bar{\mathcal{M}}$ [1]. We assume that the MDD-CF operates in the distributed manner, where nearly all the signal processing tasks, e.g., channel estimation and beamforming, are carried out locally at each AP. The CPU only sends the coded data to APs for DL transmissions or integrates the UL data received from APs via fronthaul links without requiring any channel knowledge [1]. Explicitly, such the distributed manner can make the HGNN-based model proposed in Section III more feasible and practical. In particular, the training of HGNN has to take account of message passing among all the APs and MSs, which is a quite energy-hungry process, especially when the size of MDD-CF networks is large. Meanwhile, the training of HGNN relies on the global information, and hence can only be carried out at the CPU, due to its capability of collecting the information of all nodes via the fronthaul links. In this regard, by means of the distributed operation, the CPU is able to offload the demanding signal processing tasks to APs and devotes its computational resources mainly to graph training[2].

[1]Without deviation of the main theme of this paper, we assume that, relying on the feedback of channel estimation from APs and DL/UL MSs' QoS requirements, the assignment of DL/UL subcarriers (i.e., $\mathcal{M}$ and $\bar{\mathcal{M}}$) has been determined at the CPU and fed back to APs and MSs via fronthaul before data transmission. The detailed algorithm regarding to the subcarrier assignment in MDD-based systems can be found in [22].

[2]More details with respect to the distributed operation for graph training will be presented in Remark 2.

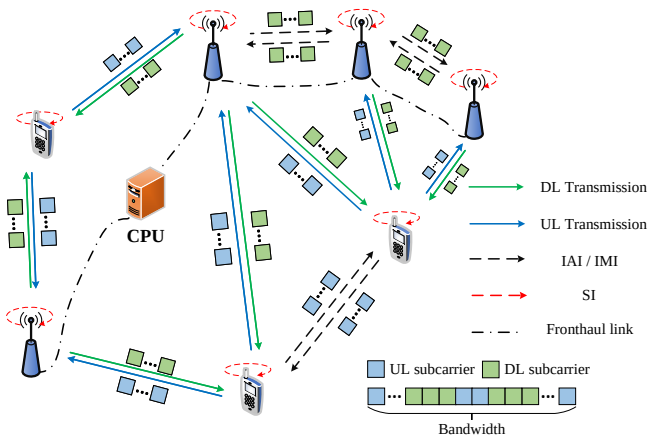

Fig. 1. Illustration of MDD-CF network.

A. Channel Model

Let $\boldsymbol{H}_{ll} \in \mathbb{C}^{N\times N}$ and h_{dd} denote the SI channels at the l-th AP and d-th MS, respectively. These two SI channels are both modeled as $(\boldsymbol{H}_{ll})_{i,j}, h_{dd} \sim \mathcal{CN}(0,1)$ [3]. Furthermore, we denote the time-domain channel impulse responses (CIRs) of the communication channels between the d-th MS and the n-th antenna at the l-th AP, the IAI channels between the n-th antenna at the l-th AP and the n'-th antenna at the l'-th AP, and the IMI channels between the d-th MS and d'-th MS by $\boldsymbol{g}_{ld}^{n} \in \mathbb{C}^{U_{ld}\times 1}$, $\boldsymbol{g}_{ll'}^{nn'} \in \mathbb{C}^{U_{ll'}\times 1}$ and $\boldsymbol{g}_{dd'} \in \mathbb{C}^{U_{dd'}\times 1}$, respectively, where $U \in \{U_{ld}, U_{ll'}, U_{dd'}\}$ is the number of taps of multipath channels. Specifically, the u-th tap of these channels is generally modeled as $(\boldsymbol{g})_u = \sqrt{\beta/U}\ \alpha_s$ with $\boldsymbol{g} \in \left\{\boldsymbol{g}_{ld}^{n}, \boldsymbol{g}_{ll'}^{nn'}, \boldsymbol{g}_{dd'}\right\}$, where $\beta \in \{\beta_{ld}, \beta_{ll'}, \beta_{dd'}\}$ accounts for the large-scale fading of path loss and shadowing. Different channel taps are assumed to be independent. Given the time-domain CIRs, the frequency-domain subcarrier channels can be obtained as $\boldsymbol{h} = \boldsymbol{F}\boldsymbol{\Psi}\boldsymbol{g}$, where $\boldsymbol{h} \in \left\{\boldsymbol{h}_{ld}^{n}, \boldsymbol{h}_{ll'}^{nn'}, \boldsymbol{h}_{dd'}\right\}$, $\boldsymbol{F} \in \mathbb{C}^{M_{\text{sum}}\times M_{\text{sum}}}$ is the FFT matrix, and $\boldsymbol{\Psi} \in \mathbb{C}^{M_{\text{sum}}\times U}$ is constructed by the first U columns of $\boldsymbol{I}_{M_{\text{sum}}}$. Moreover, the single DL/UL subcarrier channel can be expressed as $h[m] = \boldsymbol{\phi}_{\text{DL}}^{T}\boldsymbol{h}$ and $h[\bar{m}] = \boldsymbol{\phi}_{\text{UL}}^{T}\boldsymbol{h}$, respectively, where $\boldsymbol{\phi}_{\text{DL}} = \boldsymbol{I}_{M_{\text{sum}}}^{(:,m)}$ and $\boldsymbol{\phi}_{\text{UL}} = \boldsymbol{I}_{M_{\text{sum}}}^{(:,\bar{m})}$ are mapping vectors.

B. Downlink Transmission

The data transmitted on the m-th DL subcarrier for the d-th MS is denoted by $x_d[m]$, which satisfies $\mathbb{E}\left\{|x_d[m]|^2\right\} = 1$. The transmitted signal on the m-th DL subcarrier by the l-th AP is given by

$$\boldsymbol{s}_l[m] = \sum_{d\in\mathcal{D}} \sqrt{p_{ldm}}\boldsymbol{f}_{ld}[m]x_d[m], \tag{1}$$

where $\boldsymbol{f}_{ld}[m] \in \mathbb{C}^{N\times 1}$ denotes the precoding vector with $\|\boldsymbol{f}_{ld}[m]\|_2^2 = 1$, and p_{ldm} is the power allocated to the d-th MS on the m-th subcarrier. The total power budget at the l-th AP is expressed as P_l, satisfying $\sum_{m\in\mathcal{M}}\sum_{d\in\mathcal{D}} p_{ldm} \le P_l$.

The signal received from the m-th DL subcarrier by the d-th MS can be expressed as

$$y_d[m] = \sum_{l\in\mathcal{L}} \boldsymbol{h}_{ld}^{H}[m]\boldsymbol{s}_l[m] + z_d^{\text{SI}} + z_d^{\text{IMI}} + n_d, \tag{2}$$

where $n_d \sim \mathcal{CN}(0,\sigma^2)$ is the additive white Gaussian noise (AWGN). According to [23–26], the residual interference in the digital domain arising from self-interference and inter-MS interference (i.e., z_d^{SI} and z_d^{IMI} in (2)) can be modeled as Gaussian noise. Specifically, we express $z_d^{\text{SI}} \sim \mathcal{CN}(0, \xi_d^{\text{SI}}\mathbb{E}\left[\bar{z}_d^{\text{SI}}\left(\bar{z}_d^{\text{SI}}\right)^*\right])$ with $\bar{z}_d^{\text{SI}} = h_{dd}\sum_{\bar{m}\in\bar{\mathcal{M}}}\sqrt{p_{d\bar{m}}}x_d[\bar{m}]$, where $x_d[\bar{m}]$ denotes the data transmitted on the $\bar{m}$-th UL subcarrier by the d-th MS, $p_{d\bar{m}}$ denotes the transmitted power, ξ_d^{SI} denotes the level of the residual SI at MS receiver. $z_d^{\text{IMI}} \sim \mathcal{CN}(0, \xi_d^{\text{IMI}}\mathbb{E}\left[\bar{z}_d^{\text{IMI}}\left(\bar{z}_d^{\text{IMI}}\right)^*\right])$ with $\bar{z}_d^{\text{IMI}} = \sum_{d'\in\mathcal{D}\setminus\{d\}}\sum_{\bar{m}\in\bar{\mathcal{M}}}\sqrt{p_{d'\bar{m}}}h_{dd'}[\bar{m}]x_{d'}[\bar{m}]$, where ξ_d^{IMI} denotes the residual IMI level at MS d.

Based on (2), the received SINR on the m-th DL subcarrier at the d-th MS is given by

$$\text{SINR}_{d,m} = \frac{\left|\sum_{l\in\mathcal{L}}\sqrt{p_{ldm}}\boldsymbol{h}_{ld}^{H}[m]\boldsymbol{f}_{ld}[m]\right|^2}{\text{MUI}_{d,m} + \text{var}\left\{z_d^{\text{SI}}\right\} + \text{var}\left\{z_d^{\text{IMI}}\right\} + \sigma^2}, \tag{3}$$

where $\text{MUI}_{d,m} = \sum_{l\in\mathcal{L}}\sum_{d'\in\mathcal{D}\setminus\{d\}} p_{ld'm}|\boldsymbol{h}_{ld}^{H}[m]\boldsymbol{f}_{ld'}[m]|^2$ is the component of multiuser interference (MUI).

C. Uplink Transmission

The received UL signal by the l-th AP from the $\bar{m}$-th subcarrier can be expressed as

$$\boldsymbol{y}_l[\bar{m}] = \sum_{d\in\mathcal{D}} \sqrt{p_{d\bar{m}}}\boldsymbol{h}_{ld}[\bar{m}]x_d[\bar{m}] + \boldsymbol{z}_l^{\text{SI}} + \boldsymbol{z}_l^{\text{IAI}} + \boldsymbol{n}_l, \tag{4}$$

where $p_{d\bar{m}}$ denotes the power allocated by MS d to the $\bar{m}$-th UL subcarrier, which satisfies $\sum_{\bar{m}\in\bar{\mathcal{M}}} p_{d\bar{m}} \le P_d$. Similar to the received signals at MSs, the residual interferences due to the SI and IAI are modeled as Gaussian noise, where $\boldsymbol{z}_l^{\text{SI}} \sim \mathcal{CN}(0, \xi_l^{\text{SI}}\text{diag}(\mathbb{E}[\bar{\boldsymbol{z}}_l^{\text{SI}}(\bar{\boldsymbol{z}}_l^{\text{SI}})^H]))$ with $\bar{\boldsymbol{z}}_l^{\text{SI}} = \boldsymbol{H}_{ll}\sum_{m\in\mathcal{M}}\boldsymbol{s}_l[m]$, and $\boldsymbol{z}_l^{\text{IAI}} \sim \mathcal{CN}(0, \xi_l^{\text{IAI}}\text{diag}(\mathbb{E}[\bar{\boldsymbol{z}}_l^{\text{IAI}}(\bar{\boldsymbol{z}}_l^{\text{IAI}})^H]))$ with $\bar{\boldsymbol{z}}_l^{\text{IAI}} = \sum_{l'\in\mathcal{L}\setminus\{l\}}\sum_{m\in\mathcal{M}}\boldsymbol{H}_{ll'}[m]\boldsymbol{s}_{l'}[m]$, where ξ_l^{SI} and ξ_l^{IAI} denote the residual SI and IAI levels at the AP side.

Due to the distributed processing nature in our proposed system, each AP firstly processes the signal received from MSs using the local combining vectors, expressed as $\tilde{y}_l[\bar{m}] = \boldsymbol{w}_{ld}^{H}[\bar{m}]\boldsymbol{y}_l[\bar{m}]$, where $\boldsymbol{w}_{ld}[\bar{m}]$ denotes the local combining vector of AP l for detecting MS d. Then, the locally estimated data by all APs are forwarded to the CPU for final processing, which can be expressed as $y_{\text{cpu}}[\bar{m}] = \sum_{l\in\mathcal{L}}\tilde{y}_l[\bar{m}]$. It can be shown that the SINR at the CPU for detecting the data transmitted on the $\bar{m}$-th

[3] As the node's transmitter is relatively close to its receiver, compared with the distance away from other nodes, we assume that SI channel suffers from Rayleigh flat fading without any effect of path loss.

UL subcarrier of MS d can be expressed as

$$\mathrm{SINR}_{d,\bar{m}} = \frac{p_{d\bar{m}}|\tilde{\boldsymbol{w}}_d[\bar{m}]\tilde{\boldsymbol{h}}_d[\bar{m}]|^2}{\mathrm{MUI}_{d,\bar{m}} + \mathrm{SI}_{d,\bar{m}} + \mathrm{IAI}_{d,\bar{m}} + \sigma^2\left\|\tilde{\boldsymbol{w}}_d[\bar{m}]\right\|^2}, \tag{5}$$

where $\tilde{\boldsymbol{w}}_d[\bar{m}] = [\boldsymbol{w}_{1d}^H[\bar{m}], ..., \boldsymbol{w}_{Ld}^H[\bar{m}]]$, $\tilde{\boldsymbol{h}}_d[\bar{m}] = [\boldsymbol{h}_{1d}^H[\bar{m}], ..., \boldsymbol{h}_{Ld}^H[\bar{m}]]^H$, $\mathrm{MUI}_{d,\bar{m}} = \sum_{d'\in\mathcal{D}\setminus\{d\}} p_{d'\bar{m}}|\tilde{\boldsymbol{w}}_d[\bar{m}]\tilde{\boldsymbol{h}}_{d'}[\bar{m}]|^2$, $\mathrm{SI}_{d,\bar{m}} = \sum_{l\in\mathcal{L}}\mathbb{E}[\left\|\boldsymbol{w}_{ld}^H[\bar{m}]\boldsymbol{z}_l^{\mathrm{SI}}\right\|^2]$ and $\mathrm{IAI}_{d,\bar{m}} = \sum_{l\in\mathcal{L}}\mathbb{E}[\left\|\boldsymbol{w}_{ld}^H[\bar{m}]\boldsymbol{z}_l^{\mathrm{IAI}}\right\|^2]$.

Remark 1. Different from the other FD-style CF-mMIMO, e.g., IBFD-CF [3] and network-assisted full-duplex (NAFD)-based CF [24], in MDD-CF, the DL and UL transmissions occur at the same time but over orthogonal subcarrier sets in MDD-CF. Thanks to this feature, the interference is orthogonal to the desired signal in digital domain, as shown in (2) and (4). Hence, once the interference is transformed into the digital form by the analog-to-digital converter (ADC) at receiver, it can be readily removed with FFT operation. To this end, the interference cancellation of both SI and CLI in analog domain is indispensable. Otherwise, the overwhelming analog-domain power of interference leads to severe quantization noise after ADC. However, in this paper, as our main focus is on the HGNN-based power allocation method, the discussions of interference cancellation are omitted. For the readers interested in this issue, please refer to [21] for details. Instead, in this paper, we model the residual interferences as the Gaussian noise consisting of the combined effect of the additive noise introduced by automatic gain control, non-linearity of ADC and the possible phase noise generated from oscillators due to RF imperfection [23]. The parameters accounting for the residual interference levels, i.e., $\xi_l^{\mathrm{SI}}/\xi_l^{\mathrm{IAI}}$ and $\xi_d^{\mathrm{SI}}/\xi_d^{\mathrm{IMI}}$, which rely on the SI/CLI cancellation capability at APs and MSs are simply illustrated and provided in Section IV.

D. Beamforming Design

In this paper, the zero-forcing (ZF) beamforming strategy is employed for both transmitting and receiving at APs. It is well-known that the MMSE beamforming slightly outperforms the ZF beamforming in massive MIMO systems, when perfect CSI is available and especially when SINR is low [27]. However, considering the multiuser interference suppression, computation complexity as well as the concise formulation, ZF is considered in the following analysis. According to the ZF principle [28], the precoder/combiner at the l-th AP, expressed as $\boldsymbol{F}_l^{\mathrm{ZF}}[m] = [\boldsymbol{f}_{l1}^{\mathrm{ZF}}[m], ..., \boldsymbol{f}_{lD}^{\mathrm{ZF}}[m]]$ and $\boldsymbol{W}_l^{\mathrm{ZF}}[\bar{m}] = [\boldsymbol{w}_{l1}^{\mathrm{ZF}}[\bar{m}], ..., \boldsymbol{w}_{lD}^{\mathrm{ZF}}[\bar{m}]]$, can be derived as $\boldsymbol{F}_l^{\mathrm{ZF}}[m] = \boldsymbol{H}_l^H[m](\boldsymbol{H}_l[m]\boldsymbol{H}_l^H[m])^{-1}$ and $\boldsymbol{W}_l^{\mathrm{ZF}}[\bar{m}] = \boldsymbol{H}_l[\bar{m}](\boldsymbol{H}_l^H[\bar{m}]\boldsymbol{H}_l[\bar{m}])^{-1}$, respectively, where $\boldsymbol{H}_l[m] = [\boldsymbol{h}_{l1}[m], ..., \boldsymbol{h}_{lD}[m]]^H$ and $\boldsymbol{H}_l[\bar{m}] = [\boldsymbol{h}_{l1}[\bar{m}], ..., \boldsymbol{h}_{lD}[\bar{m}]]$. Note that, in order to ensure that the MUI is fully suppressed, the implementation of ZF beamforming should adhere to the constraint of $N \geq D$ [4]. In this case, the MUI terms in (3) and (5) are equal to zero. Therefore, the $\mathrm{SINR}_{d,m}$ and $\mathrm{SINR}_{d,\bar{m}}$ can be rewritten as

$$\begin{aligned}\mathrm{SINR}_{d,m} &= \frac{|\sum_{l\in\mathcal{L}}\sqrt{p_{ldm}}\omega_{ldm}|^2}{\xi_d^{\mathrm{SI}}\Theta_{\mathrm{DL}} + \sigma^2},\\ \mathrm{SINR}_{d,\bar{m}} &= \frac{p_{d\bar{m}}L^2}{\sum_{l\in\mathcal{L}}\upsilon_{ld\bar{m}}(\xi_l^{\mathrm{SI}}\Theta_{\mathrm{UL}} + \sigma^2)},\end{aligned} \tag{6}$$

where $\omega_{ldm} = 1/\|\boldsymbol{f}_{ld}^{\mathrm{ZF}}[m]\|_2$, $\upsilon_{ld\bar{m}} = \|\boldsymbol{w}_{ld}^{\mathrm{ZF}}[\bar{m}]\|_2^2$, $\Theta_{\mathrm{DL}} = \sum_{\bar{m}\in\bar{\mathcal{M}}} p_{d\bar{m}} + \sum_{d'\in\mathcal{D}\setminus\{d\}}\sum_{\bar{m}\in\bar{\mathcal{M}}}(\xi_d^{\mathrm{IMI}}\beta_{dd'}p_{d'\bar{m}}/\xi_d^{\mathrm{SI}}M_{\mathrm{sum}})$ and $\Theta_{\mathrm{UL}} = \sum_{m\in\mathcal{M}}\sum_{d\in\mathcal{D}} p_{ldm} + \sum_{l'\in\mathcal{L}\setminus\{l\}}\sum_{m\in\mathcal{M}}\sum_{d\in\mathcal{D}}(\xi_l^{\mathrm{IAI}}\beta_{ll'}p_{l'dm}/\xi_l^{\mathrm{SI}}M_{\mathrm{sum}})$.

E. Problem Formulation

In our proposed MDD-CF system, as both APs and MSs operate in the MDD mode, the DL and UL transmissions are strongly coupled in the same frequency band and time slot. For example, as shown in (6), the power allocated to DL (UL) will also cause interference to UL (DL) data reception. To this end, like any other FD-style systems, the optimization problem in MDD-CF should jointly consider DL and UL with the objective to maximize the system's total SE. Nevertheless, the peculiarity of MDD-CF is that, it enables the FD operation via transmitting DL and UL signals over two orthogonal subcarrier sets. Accordingly, the SE expression can be formulated as $\Lambda_{\mathrm{SE}} = \frac{1}{M_{\mathrm{sum}}}\sum_{d\in\mathcal{D}}\big(\sum_{m\in\mathcal{M}}\ln(1+\mathrm{SINR}_{d,m}) + \sum_{\bar{m}\in\bar{\mathcal{M}}}\ln(1+\mathrm{SINR}_{d,\bar{m}})\big)$, where $\mathrm{SINR}_{d,m}$ and $\mathrm{SINR}_{d,\bar{m}}$ are provided in (6). Therefore, the overall optimization problem can be stated as:

$$\max_{p_{ldm},p_{d\bar{m}}} \quad \Lambda_{\mathrm{SE}} \tag{7a}$$

$$\text{s.t.} \quad \sum_{m\in\mathcal{M}}\sum_{d\in\mathcal{D}} p_{ldm} \leq P_l,\ \forall l\in\mathcal{L}, \tag{7b}$$

$$\sum_{\bar{m}\in\bar{\mathcal{M}}} p_{d\bar{m}} \leq P_d,\ \forall d\in\mathcal{D}, \tag{7c}$$

$$\sum_{m\in\mathcal{M}} \ln(1+\mathrm{SINR}_{d,m}) \geq \chi_{\mathrm{DL}},\ \forall d\in\mathcal{D}, \tag{7d}$$

$$\sum_{\bar{m}\in\bar{\mathcal{M}}} \ln(1+\mathrm{SINR}_{d,\bar{m}}) \geq \chi_{\mathrm{UL}},\ \forall d\in\mathcal{D}. \tag{7e}$$

In the above formulas, the constraints (7b) and (7c) imply that the transmit power at APs and MSs is subject to their maximum power budgets. Moreover, as DL and UL are simultaneously operated, the inter-AP interference and inter-MS interference may result in the unsatisfied performance at the MSs with relatively poor channel conditions. Hence, to guarantee the fairness to a certain extent, the constraints (7d) and (7e) are applied to make sure that all the MSs can attain at least the predefined minimum DL and UL rates χ_{DL} and χ_{UL}.

It can be observed that (7) is a NP-hard nonconvex problem with the nonconvex constraints as shown in (7d)

[4]We will discuss the case of $D \gg N$ in Section IV-D along with the user-centric clustering algorithm.

and (7e). Generally, to solve this kind of complicated problems, we have to transform the main optimization function as well as the constraints into the approximated convex ones, and then solve them in an iterative way. With this consideration, in this paper, we propose a QT-SCA method, which can be found in detail in Appendix A. Unfortunately, the complexity of QT-SCA increases significantly as the size of network becomes large, especially when the multicarrier FD-like systems, such as our proposed MDD-CF system, are considered. To this end, we resort to the GNN to solve this optimization problem, which will be demonstrated to exhibit low complexity and high efficiency.

III. Graph Learning in MDD-CF networks

In order to leverage the structural information of MDD-CF network to solve the complicated problem, as that formulated in (7), the heterogeneous graph learning based PA scheme is introduced. We aim to learn a scalable and transferable heterogeneous graph neural network to efficiently distribute both APs' and MSs' transmit power to maximize the SE of the distributed MDD-CF systems.

A. Definition of Heterogeneous Graph

A heterogeneous graph can be represented as $G = (\mathcal{V}, \mathcal{E})$, where $\mathcal{V}$ is the set of nodes, and $\mathcal{E}$ is the set of edges. The heterogeneous graph has a node type mapping function $\phi : \mathcal{V} \longrightarrow \mathcal{Q}$ and an edge type mapping function $\psi : \mathcal{E} \longrightarrow \mathcal{P}$, where $\mathcal{Q}$ and $\mathcal{P}$ denote the sets of predefined node types and link types, $|\mathcal{Q}|+|\mathcal{P}| > 2$ [29]. Explicitly, we can write $\mathcal{Q} = \{Q_1, Q_2, ...\}$ and $\mathcal{P} = \{P_1, P_2, ...\}$, where Q_i and P_j are the i-th node type and j-th link type. Let $\boldsymbol{v}_i \in \mathbb{R}^{F_v \times 1}$ denote a node with F_v-dimensional features and $\boldsymbol{e}_{i,j} = (\boldsymbol{v}_i, \boldsymbol{v}_j) \in \mathbb{R}^{F_e \times 1}$ denote an edge pointing from $\boldsymbol{v}_j$ to $\boldsymbol{v}_i$, which has F_e-dimensional features. Given the mapping function ϕ and ψ, each node belongs to a particular node type of $\phi(\boldsymbol{v}) \in \mathcal{Q}$ and each edge belongs to a specific relation of $\psi(\boldsymbol{e}) \in \mathcal{P}$. The neighborhood of a node $\boldsymbol{v}_i$ is defined as $\mathcal{N}_i = \{\boldsymbol{v}_j \in \mathcal{V} | \boldsymbol{e}_{i,j} \in \mathcal{E}\}$.

Furthermore, in a heterogeneous graph, two nodes may be connected via different paths. For example, an AP and an MS in the FD-based networks may be connected via two paths, namely the AP-DL-MS and MS-UL-AP paths, and these paths are denoted as meta-paths [30]. Theoretically, a meta-path Φ is defined in the form of $Q_1 \xrightarrow{P_1} Q_2 \xrightarrow{P_2} \cdots \xrightarrow{P_n} Q_{n+1}$, which explains a composite relation $P = P_1 \circ P_2 \circ \dots P_n$ from node type Q_1 to node type Q_{n+1}, where $\circ$ denotes the composition operator on relations. It is noteworthy that depending on the definition of meta-path, the relation between two nodes in the heterogeneous graph may have different semantics. For instance, AP-DL-MS means an AP transmits signal to an MS via DL channel, while MS-UL-AP means an MS transmits signal to an AP via UL channel. Once a meta-path Φ is given, the specific meta-path based neighbors $\mathcal{N}_i^{\Phi}$ of node $\boldsymbol{v}_i$ can be obtained, which is defined as the set of nodes connected with $\boldsymbol{v}_i$ via the meta-path Φ.

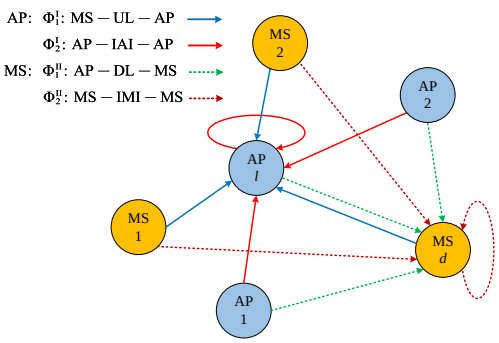

Fig. 2. An exemplified graph of CF network.

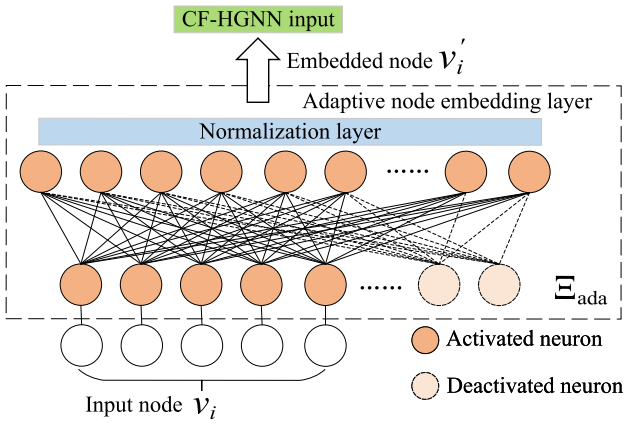

Fig. 3. Adaptive node embedding layer.

B. Heterogeneous Graph for MDD-CF Networks

Intuitively, as shown in Fig. 2, it is straightforward to model an MDD-CF network as a heterogeneous graph. It can be observed from the figure that there are two types of nodes, namely AP and MS, each of which is associated with two meta-paths. Specifically, for AP l, all MSs are connected with it via the meta-path Φ_1^{I} (MS-UL-AP), and the remaining APs are connected with it via the meta-path Φ_2^{I} (AP-IAI-AP). Note that, the SI caused by AP l itself is classified into Φ_2^{I} by adding a self-loop. Similarly, the meta-paths Φ_1^{II} and Φ_2^{II} associated with MS d are AP-DL-MS and MS-IMI-MS, respectively.

In the heterogeneous graph of MDD-CF, the node feature vectors of AP l and MS d are defined as

$$\begin{aligned} \boldsymbol{v}_l &= \left[\boldsymbol{\omega}_{l1}^T ... \boldsymbol{\omega}_{lM}^T, P_l, \xi_l^{\mathrm{SI}}, \xi_l^{\mathrm{IAI}}\right]^T \in \mathbb{R}^{(DM+3)\times 1}, \\ \boldsymbol{v}_d &= \left[\boldsymbol{\upsilon}_{1d}^T ... \boldsymbol{\upsilon}_{\bar{M}d}^T, P_d, \xi_d^{\mathrm{SI}}, \xi_d^{\mathrm{IMI}}\right]^T \in \mathbb{R}^{(L\bar{M}+3)\times 1}, \end{aligned} \tag{8}$$

respectively, where $\boldsymbol{\omega}_{lm} = [\omega_{l1m}, ..., \omega_{lDm}]^T$ is the m-th DL equivalent subchannel gains between AP l and all the D MSs, and $\boldsymbol{\upsilon}_{\bar{m}d} = [\upsilon_{1d\bar{m}}, ..., \upsilon_{Ld\bar{m}}]^T$ is the $\bar{m}$-th UL equivalent subchannel gains between MS d and all the L APs, when the ZF beamforming shown in (6) is applied. Moreover, to simplify the model for the sake of reducing complexity, the attribute of edges is assumed to be the Euclidean distance between any two nodes, expressed as $e_{i,j} = d_{i,j}, \forall i, j \in \mathcal{V}$. If $i = j, e_{i,j} = 0$ denotes the edge

feature of self-loop.

Remark 2. In the distributed MDD-CF systems, each AP equipped with a baseband processor is able to independently implement channel estimation and DL/UL beamforming, while the CPU only needs to collect the processed signals from APs and then accomplish the final data detection. Hence, in order to fully exploit the APs' computational potentials while avoiding using long-stacked channel vectors as node features, we assume that, each AP first computes the equivalent DL/UL subchannel gains based on the estimated channel state information (CSI). Then, the equivalent DL/UL subchannel gains are transmitted to the CPU as the AP/MS node features. All these are done during the offline graph training[5]. Note that in some references, such as [31], the authors used the geographic location information (GLI) as the input of the learning-based network to reduce the training overhead. This approach has the advantage that the low-dimensional coordinate values of AP/MS can be directly used as node features without requiring to computing beamformers. However, in MDD-based systems, power needs to be allocated among different subcarriers, while the GLI lacks not only the small-scale information of the involved communication channels but also the multi-antenna characteristics of MIMO systems. Explicitly, the GLI is unable to provide the required information and hence, is infeasible in MDD-based systems.

C. Heterogeneous Graph Learning Assisted Power Allocation in MDD-CF Networks

In this subsection, we formally present the CF-HGNN to solve the PA problem in MDD-CF networks. The architecture of CF-HGNN consists of four components: 1) adaptive node embedding; 2) meta-path based message passing; 3) meta-path based attention; 4) downstream PA learning. The overall CF-HGNN is type-specific and the parameters for processing AP and MS nodes are not shared.

1) Adaptive Node Embedding: In general, in order to guarantee the scalability of GNN, the size of node feature should be irrelevant to the number of nodes involved. As seen in (8), the feature dimensions of input nodes are related to L, D and $M/\bar{M}$, which vary with respect to the scales of CF networks. Therefore, if the CF networks with the size of $S_1 = \left(D_1, L_1, M_1, \bar{M}_1\right)$ are selected as the training samples, the trained CF-HGNN model can not be generalized to the CF networks with the different size of $S_2 = \left(D_2, L_2, M_2, \bar{M}_2\right)$, due to the inconsistent sizes of node feature. Hence, the dimensions of node feature should be fixed for the sake of scalability and transferability. With this in mind, we propose an adaptive node embedding layer, which can handle the graph nodes with varying input feature dimensions through adaptively activating or deactivating the neurons in the multi-layer perceptron (MLP), i.e., $\Xi_{\text{ada}}(\boldsymbol{v}_l)$ and $\Xi_{\text{ada}}(\boldsymbol{v}_d)$, as depicted in Fig. 3. Specifically, before the normalization layer, AP and MS nodes are transformed by two embedding matrices, which are expressed as

$$\boldsymbol{v}_l^{'} = \boldsymbol{W}_{\text{AP}}^{(:,1:DM+3)}\boldsymbol{v}_l,\ \boldsymbol{v}_d^{'} = \boldsymbol{W}_{\text{MS}}^{(:,1:L\bar{M}+3)}\boldsymbol{v}_d, \tag{9}$$

where $\boldsymbol{W}_{\text{AP}} \in \mathbb{R}^{F_{\text{AP}}^{'} \times F_{\text{AP}}}$ and $\boldsymbol{W}_{\text{MS}} \in \mathbb{R}^{F_{\text{MS}}^{'} \times F_{\text{MS}}}$ map different AP and MS input nodes into two feature domains with predefined sizes of $F_{\text{AP}}^{'}$ and $F_{\text{MS}}^{'}$. Note that, as the ZF beamforming is applied, the maximum input size of the embedding layer for AP nodes is subject to the number of antennas employed at individual AP, having the relationship of $F_{\text{AP}} = NM + 3$. In the context of MS, we assume $F_{\text{MS}} = L^{'}\bar{M} + 3$, where $L^{'}$ denotes the maximum number of APs that can be deployed in a CF network within a certain area. Additionally, to make the model also generalized to the various numbers of subcarriers, the M and $\bar{M}$ can be pre-defined as a relative large value.

Remark 3. In Section II-D, we assumed that, in our proposed distributed MDD-CF system, each AP having $N \geq D$ antennas individually communicates with all the D MSs using ZF beamforming. In this case, the above-mentioned embedding layer imposes strict limitation on the maximum number of MSs, which should not exceed the number of antennas configured at each AP. However, if MSs are densely distributed or each AP is only equipped with a small number of antennas, the AP node features can no longer be set as (8), as the zero-forcing beamforming cannot be achieved in the case of $D > N$ [6]. Moreover, in the above model, the number of APs is restricted to $L^{'}$, meaning that the CF-HGNN cannot be generalized to the CF networks with more than $L^{'}$ APs [7]. In these cases, to guarantee the scalability of CF-HGNN and reduce the computational complexity, one possible approach is to transform the dense graph into the sparse graph with the aid of user-centric clustering [1]. For instance, if ZF beamforming is used, each AP can concurrently serve up to N MSs depending on the channel conditions [8], and the graph is then updated with only connecting AP with a small number of MSs instead of all the MSs. In doing so, the dimensions of the AP node features are subject

[5]In principle, apart from ZF, the beamforming methods, such as MMSE or matched filtering, may also be employed. If the number of antennas at individual AP and the numbers of MSs and subcarriers are small, it is possible to represent the AP and MS node features by their channel vectors, which have the size of $(2DNM + 3)$ and $(2LN\bar{M}+3)$, respectively, when both the real and imaginary parts of the complex vectors are considered. Correspondingly, the beamforming vectors associated with PA can be directly learned at the final output layer, rather than choosing one of the known beamforming schemes to generate the network inputs. However, if the numbers of antennas at each AP, MSs and subcarriers are large, the huge dimensions of node features will make the model extremely hard to train.

[6]Although the MMSE beamforming can be applied in the case of $D > N$, the increasing number of MSs leads to large multiuser interference and high dimensions of AP node features.

[7]In principle, $L^{'}$ can be predefined to a sufficiently large number so as to make CF-HGNN scalable to the network with densely distributed APs. However, in doing so, it will significantly increase the training overhead of the CF-HGNN.

[8]There are many sub-optimal user-centric clustering algorithms in the open literature, and the most widely used method is based on the large-scale fading coefficient among APs and MSs [32].

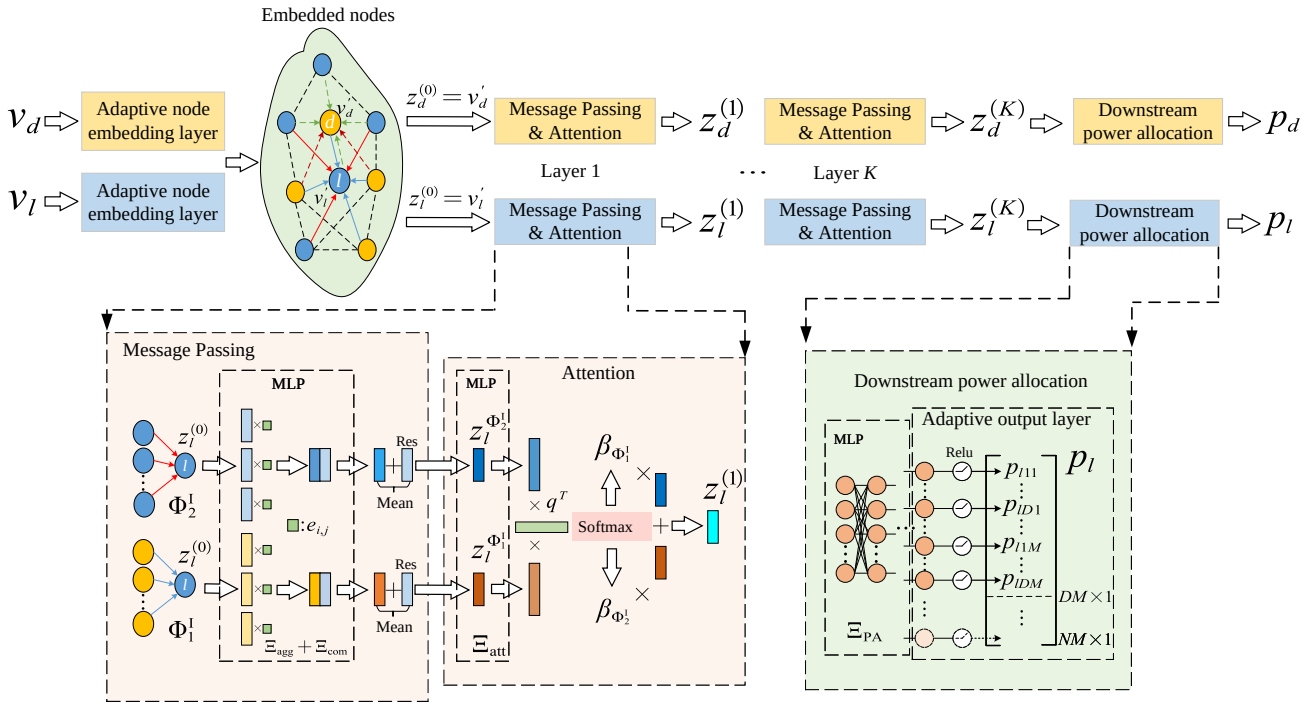

Fig. 4. The overall architecture of CF-HGNN network.

to the number of antennas, while that of the MSs node features are only relied on a fraction of APs. Hence, our node feature definition of (8) is still applicable. In Section IV-D, we will present an example accounting for the user-centric clustering.

2) Meta-Path Based Message Passing: According to the example shown in Fig. 2, each AP/MS node connects with its neighboring nodes via two independent meta-paths. Hence, within a meta-path Φ, the process of message passing from the neighboring nodes to node $i \in \{l, d\}$ itself can be divided into the following two steps:

(i) **Aggregation**: The node feature of all the nodes connected to node i via meta-path Φ and the feature of interconnection edges are first aggregated and then averaged to obtain the neighboring information of node i, which can be expressed as

$$\boldsymbol{v}_{i,j}^{'} = \frac{1}{|\mathcal{N}_i^{\Phi}|}\Xi_{\text{agg}}\Big(\sum_{j\in\mathcal{N}_i^{\Phi}} \boldsymbol{v}_j^{'} \cdot e_{i,j}\Big) \tag{10}$$

where Ξ_{agg} is an aggregator composed of the fully-connected, activation and normalization layers.

(ii) **Combination with Residual Block**: To obtain the meta-path based embedding of node i, the node feature of node i and the neighbors' projected features are combined by a combiner Ξ_{com}. Additionally, in order to avoid the degradation of the original node feature after multi-layer message passing, a simple residual block is included, which calculates the element-wise Mean$(\cdot)$ between the post-combined and the original node features. The above-described process can be expressed as

$$\boldsymbol{z}_i^{\Phi} = \text{Mean}\left(\Xi_{\text{com}}\left(\boldsymbol{v}_i^{'} \oplus \boldsymbol{v}_{i,j}^{'}\right) + \underbrace{\boldsymbol{v}_i^{'}}_{\text{Res}}\right) \tag{11}$$

where Ξ_{com} has the same structure as Ξ_{agg}, $\oplus$ is the concatenation operation, and $\boldsymbol{v}_i^{'}$ denotes the residual connection.

Through the Aggregation and Combination, each AP/MS can not only collect the information from both the communication nodes and interference sources, but also partly maintain its original information during the message passing process, which is essential for fulfilling the following power allocation task.

3) Meta-Path Based Attention: In general cases, the information update of node i is the summation of the message collected from all the meta-paths with the same coefficients, expressed as $\boldsymbol{z}_i = \sum_{\Phi} \boldsymbol{z}_i^{\Phi}$. However, in MDD-CF networks, since AP/MS nodes receive information via both the interfering path and data transmission path, it is intuitive that these two meth-paths may has quite different impact on the information integration. For instance, if an AP node is closely surrounded by MS nodes but the other AP nodes are far away from it, the meta-path Φ_1^{I} should be more important than Φ_2^{I}. Based on this observation, we propose the meta-based attention in CF-HGNN to enable the GNN to automatically learn the importance of the two meta-paths. An example of calculating the attention

$$\mathcal{L}(\boldsymbol{\theta}) = \mathbb{E}\Bigg[-\Lambda_{\mathrm{SE}} + \sum_{d=1}^{D} \Bigg(\kappa_1 \mathrm{Relu}\big(\chi_{\mathrm{DL}} - \sum_{m\in\mathcal{M}} \ln(1+\mathrm{SINR}_{d,m})\big) + \kappa_2 \mathrm{Relu}\big(\chi_{\mathrm{UL}} - \sum_{\bar{m}\in\bar{\mathcal{M}}} \ln(1+\mathrm{SINR}_{d,\bar{m}})\big) + \kappa_3 \mathrm{Relu}\big(\sum_{\bar{m}\in\bar{\mathcal{M}}} p_{d\bar{m}} - P_d\big)\Bigg) + \sum_{l=1}^{L} \kappa_4 \mathrm{Relu}\big(\sum_{m\in\mathcal{M}} \sum_{d\in\mathcal{D}} p_{ldm} - P_l\big)\Bigg] \tag{14}$$

vector of an AP node is as follows [33]:

$$\alpha_{\Phi_1^{\mathrm{I}}} = \frac{1}{L} \sum_{l\in\mathcal{L}} \boldsymbol{q}^T \Xi_{\mathrm{att}}(\boldsymbol{z}_l^{\Phi_1^{\mathrm{I}}}),\ \beta_{\Phi_1^{\mathrm{I}}} = \frac{\exp(\alpha_{\Phi_1^{\mathrm{I}}})}{\exp(\alpha_{\Phi_1^{\mathrm{I}}}) + \exp(\alpha_{\Phi_2^{\mathrm{I}}})}, \tag{12}$$

where Ξ_{att} is the MLP layer for attention, $\boldsymbol{q}$ is the learnable attention vector, $\boldsymbol{z}_l^{\Phi_1^{\mathrm{I}}}$ denotes the aggregated information via meta-path Φ_1^{I}. Then, the final node representation of AP l is $\boldsymbol{z}_l = \beta_{\Phi_1^{\mathrm{I}}} \boldsymbol{z}_l^{\Phi_1^{\mathrm{I}}} + \beta_{\Phi_2^{\mathrm{I}}} \boldsymbol{z}_l^{\Phi_2^{\mathrm{I}}}$, where $\boldsymbol{z}_l \in \mathbb{R}^{F'_{\mathrm{AP}}\times 1}$. Similarly, $\boldsymbol{z}_d \in \mathbb{R}^{F'_{\mathrm{MS}}\times 1}$ at MS d can be obtained. It is noteworthy that the process of message passing plus attention can be iteratively implemented for K times by initializing $\boldsymbol{z}_l^{(0)} = \boldsymbol{v}'_l$ and $\boldsymbol{z}_d^{(0)} = \boldsymbol{v}'_d$, so as to collect the information from high-hop neighbors. Owing to this, our proposed model can also be termed as the K-layer CF-HGNN.

4) Downstream Power Allocation Learning: After the K-th iteration, the final representation of AP and MS nodes, i.e., $\boldsymbol{z}_l^{(K)}$ and $\boldsymbol{z}_d^{(K)}$, are used for the downstream PA learning, which can be expressed as:

$$\begin{aligned} \boldsymbol{p}_l \in \mathbb{R}^{DM\times 1} &= \mathrm{Relu}\Big(\Xi_{\mathrm{PA}}(\boldsymbol{z}_l^{(K)})^{(1:DM)}\Big), \\ \boldsymbol{p}_d \in \mathbb{R}^{\bar{M}\times 1} &= \mathrm{Relu}\Big(\Xi_{\mathrm{PA}}(\boldsymbol{z}_d^{(K)})\Big), \end{aligned} \tag{13}$$

where Ξ_{PA} denotes the MLP for PA learning, and $\mathrm{Relu}(\cdot)$ is used to constrain the power to be positive. Corresponding to the adaptive node embedding considered in part 1), in order to make it feasible for the network with different number of MSs, the adaptive output layer can support the PA for up to NM elements by activating or deactivating the neurons. By contrast, for UL PA, provided that the number of available UL subcarriers is fixed, the size of the output layer for MS node remains to $\bar{M}$, as each MS only needs to allocate UL power.

The overall architecture of the CF-HGNN for an AP node is shown in Fig. 4, which is the same for MS nodes, except the different size of output layer as above-mentioned. Note that all the MLPs shown in Fig. 4 are AP-specific, which means that the MLPs for MSs are different from that for APs.

Finally, to perform the CF-HGNN training in an unsupervised way, we define the loss function as in (14), shown on the top of this page, where $\boldsymbol{\theta}$ denotes all the parameters of the neural network, κ_i denotes the weighted factor, and the expectation is taken with respect to the channel realizations. In (14), each ReLU penalty term has a positive value, only if the DL/UL QoS requirements and transmit power budgets are not satisfied. This will enforce the training process towards satisfying the given requirements. Additionally, in (14), the positive parameters κ_i give different priorities to the penalty terms.

During the offline training stage, we first generate the training samples of random MDD-CF networks in the form of epochs. Within each epoch, the training samples are divided into multiple mini-batch sets using data shuffling to avoid over/underfitting. Then, the updates of the model parameters $\boldsymbol{\theta}$ over a mini-batch are achieved by the Adam optimizer with a fixed learning rate [34]. The training of CF-HGNN is implemented with a maximum 200 of epochs, with early stopping. During the test stage, the well-trained model can be directly utilized to a new MDD-CF network to realize the online power allocation, by means of the linear matrix multiplications, as described in (9) - (13).

IV. Simulation Results and Analysis

A. Simulation Setup

The large-scale fading model is given by [1]:

$$\beta[\mathrm{dB}] = -30.5 - 36.7\log_{10}(d) + \sigma_{\mathrm{sh}} z, \tag{15}$$

where d denotes the distance between any two nodes, $\sigma_{\mathrm{sh}} z$ is the shadowing fading with a standard deviation of $\sigma_{\mathrm{sh}} = 4$ dB and $z \sim \mathcal{N}(0,1)$. Furthermore, we assume that APs are capable of providing 30 dB of IAI suppression in the propagation/analog domain by employing the existing approaches, such as antenna cross-polarization, beam separation and absorber [35]. Then, assume that the 12-bit ADCs are applied, the MDD system can suppress IAI up to 72 dB (i.e., $\xi_l^{\text{MDD-IAI}} = -72$ dB, $\forall l$, in (4)), of which 42 dB is attributed to the digital-domain cancellation by FFT [9]. By contrast, as MSs are lightweight equipments with single antenna and can hardly share channel knowledge with other MSs, they cannot actively suppress IMI. However, similar to APs, MSs are able to cancel 42 dB IMI in the digital domain (i.e., $\xi_d^{\text{MDD-IMI}} = -42$ dB, $\forall d$, in (2)) with the aid of the FFT operation [23]. Unless otherwise noted, the simulation parameters of the MDD-CF network are listed in Table II.

As for the settings of the neural network, we adopt a 2-layer CF-HGNN based on Pytorch Geometric [36]. The general MLPs Ξ_{agg} and Ξ_{com} in (10) and (11) during the message passing stage contains multiple fully-connected linear layers followed by the LeakyRelu activation layer and batch normalization layer. By contrast, the Ξ_{PA} in

[9]The 12-bit ADC has a maximum dynamic range of 42dB, which means it can accommodate up to 42 dB of power of IAI, and transform it into digital signal without extra quantization noise [35].

TABLE I
ARCHITECTURE OF INVOLVED MLPS

MLPs	AP		MS	
	AP-IAI-AP	MS-UL-AP	MS-IMI-MS	AP-DL-MS
Ξ_{agg}	$64 \times 256 \times 512$	$128 \times 256 \times 512$	$128 \times 256 \times 512$	$64 \times 256 \times 512$
Ξ_{com}	$576 \times 1024 \times 64$	$576 \times 1024 \times 64$	$640 \times 1024 \times 128$	$640 \times 1024 \times 128$
Ξ_{ada}	$F_{\text{AP}} \times 64$		$F_{\text{MS}} \times 128$	
Ξ_{att}	64×64		128×128	
Ξ_{PA}	$64 \times 256 \times 512 \times DM$		$128 \times 256 \times \bar{M}$	

TABLE II
SIMULATION PARAMETERS

Default parameters	Value
Cell area ($S_{\text{D}} \times S_{\text{D}}$)	$(400 \times 400)\text{m}^2$
Number of antennas per AP (N)	8
Number of DL/UL subcarriers ($M, \bar{M}$)	(4, 2)
AP and MS power ($P_l, P_d, \forall l, d$)	(40, 30) dBm
QoS requirements ($\chi_{\text{DL}}, \chi_{\text{UL}}$)	(0.5, 0.1) nats/s/Hz
Noise power (σ^2)	-94 dBm
Delay taps (U)	4
Residual SI level at AP ($\xi_l^{\text{SI}}, \forall l$)	-120 dB
Residual SI level at MS ($\xi_d^{\text{SI}}, \forall d$)	-110 dB

(13) is employed with multiple fully-connected linear layers without batch normalization layer. Moreover, the Ξ_{ada} in (9) is a single-layer MLP with one fully-connected linear layer followed by one batch normalization layer with the settings of $F_{\text{AP}}^{'} = 64$ and $F_{\text{MS}}^{'}$=128 [10], while the Ξ_{att} in (12) is a single-layer MLP with only one fully-connected linear layer. The sizes of above-mentioned MLPs are listed in Table I. Furthermore, we empirically set κ_i in (14) as $\{0.1, 1, 0.1, 0.1\}$ during training. To optimize the CF-HGNN, we adopt the Adam optimizer with a learning rate of 0.001. For data preparation, as the involved data, e.g., subchannel gains and transmit power, have non-identical distributions with different scales, the data normalization is necessary in this case. Specifically, we use the Z-score normalization method to separately pre-process the subchannel gains of node feature and Euclidean distance of edge feature [37]. Additionally, the data of transmit power and interference cancellation capabilities are separately pre-processed by max-min normalization.

Moreover, we randomly generate 10000 and 1000 CF network layout samples for training and testing, respectively, under the assumption that APs and MSs are uniformly distributed within a square area of $(S_D \times S_D)\text{m}^2$. The batch size for training is 64, and the network parameters are only updated during training, which stay constant during testing. The CF-HGNN is run on a GeForce GTX laptop 3080Ti, while the other algorithms are implemented on the 12th Gen Intel(R) Core(TM) i7-12700H 2.70 GHz [11].

[10]The settings of $F_{\text{AP}}^{'}/F_{\text{MS}}^{'}$ are critical to the achievable performance of CF-HGNN. Too small or too large values may lead to the performance degradation. In our future research, we will further investigate the impact and optimization of the hyperparameters, such as $F_{\text{AP}}^{'}/F_{\text{MS}}^{'}$, so as to improve the performance of CF-HGNN.

[11]The codes for generating the results are available at https://github.com/bhli168/MDD_GNN.

B. Performance Comparison

In this section, we make a comprehensive performance comparison between different PA methods in MDD-CF networks, where the numbers of MSs and APs are fixed during training and testing, and set to $L = 24$ and $D = 6$, respectively. In this case, the embedding matrices in Ξ_{ada} and Ξ_{PA} act as identical matrices and are not learnable.

The following benchmark schemes are considered in our study:

- QT-SCA: As far as we know, there is no feasible optimization method in the open literature, which can be directly applied to the FD-style multicarrier CF-mMIMO systems. Hence, we leverage our proposed QT-SCA as a non-learning benchmark scheme, which is implemented using the CVX tool [38].
- Greedy unfair: The water-filling algorithm is used by each AP/MS to distribute its power to the DL/UL subcarriers, regardless of the QoS constraints [39].
- FC-DNN: It is a fully-connected DNN [40]. To adopt FC-DNN, the DL/UL equivalent subchannel gains are vertically stacked as the input vector $\boldsymbol{v} \in \mathbb{C}^{LD(M+\bar{M})}$.
- CNN: It is the CNN designed for TDD-CF systems [11]. To make it compatible in MDD-CF systems for simultaneous DL and UL power allocation, the DL/UL equivalent subchannel gains are used to construct the 3D input matrix $\boldsymbol{V}$, which has the size of $(L, D, M + \bar{M})$.
- HGNN: It is a basic heterogeneous GNN model inspired by [18], where only heterogeneous nodes (i.e., APs and MSs) are included, while all the edges are homogeneous. Additionally, we assume that the HGNN has the same aggregation and combination structures as our proposed CF-HGNN. To train the HGNN, the node features of APs and MSs are pre-processed to the same size, and the embedding output layer is leveraged to generate different power vectors for APs and MSs.

Firstly, we compare the various power allocation methods in terms of the SE distribution obtained from 1000 testing CF network layouts. As shown in Fig. 5(a), the CF-HGNN achieves nearly the same performance as the QT-SCA in terms of the 95%-likely SE. The HGNN lags behind the CF-HGNN, due to that it treats the interference and communication paths equally during message passing, and take no account of attention mechanism. Furthermore, as the FC-DNN and CNN can only process the vectors or matrices of the equivalent subchannel gains and are unable to exploit the structure of CF networks, their

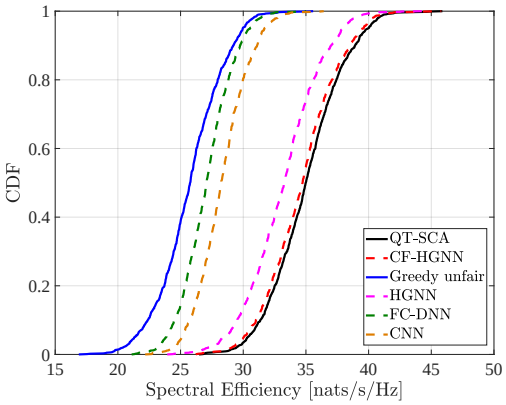

(a) Cumulative distribution of SE

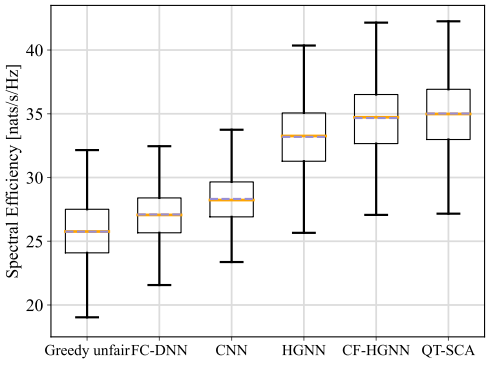

(b) Box plots of SE

Fig. 5. Performance comparison between various PA methods, when MDD-CF has $L = 24$ APs and $D = 6$ MSs.

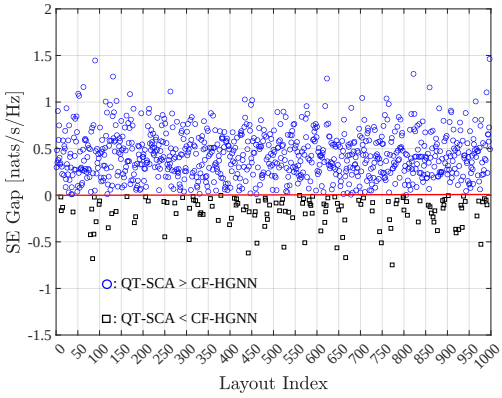

(a) Cumulative distribution of SE

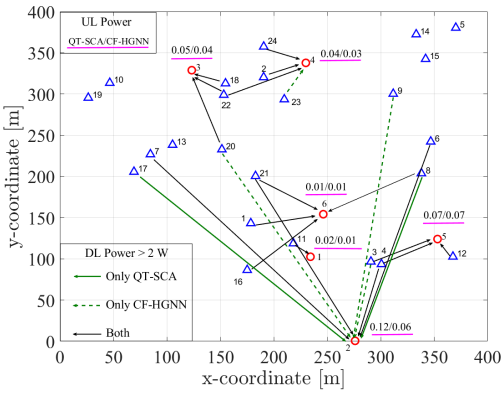

(b) An MDD-CF network topology

Fig. 6. Performance comparison of QT-SCA and CF-HGNN, when MDD-CF has $L = 24$ APs and $D = 6$ MSs.

performance in terms of 95%-likely SE is far below that attained by the GNN-based and QT-SCA methods. More explicitly, as shown in Fig. 5(b), the CF-HGNN and QT-SCA outperform the other methods in terms of SE. In particular, as seen from Fig. 5(b), the FC-DNN and CNN have relatively narrow range of SE distribution, implying that these two methods are insensitive to the various network structures. Moreover, the greedy unfair method has the worst SE performance. The rationale behind is that although the greedy unfair method can maximize the SE of the classic half-duplex based multiuser systems [39], it lacks the capability to manage the complicated interference in the FD-style systems, hence leading to the poor performance at both APs and MSs. By contrast, the learning-based and QT-SCA methods are capable of taking account of interference in their loss functions or optimization formulation, which enable them to achieve better performance than the greedy unfair method.

Then, we will look deeper into the performance comparison between QT-SCA and CF-HGNN[12]. In Fig. 6(a), the SE performance gaps between the QT-SCA and CF-HGNN with regard to 1000 testing network layouts are depicted. It can be observed that the absolute SE gaps between these two methods are lower than 1.5 nats/s/Hz. Furthermore, there are several layouts, where the CF-HGNN outperforms the QT-SCA, which reflects that the CF-HGNN is capable of learning the near-optimal solutions for PA in MDD-CF networks. Furthermore, in Fig. 6(b), we randomly select one of the CF network layouts used in the testing samples to investigate the detailed PA results attained by the QT-SCA and CF-HGNN. To make the drawing clear in Fig. 6(b), the DL connections with transmit power less than $2W$ are omitted, and different colored lines are used to denote the DL connections obtained by either methods or by both. It is not surprise that, as Fig. 6(b) shows, except MS 2, both the CF-HGNN and QT-SCA yield the same subset of the major serving APs for each of MSs, and also obtain the similar results of UL PA. As for MS 2, since it locates relatively far away from APs, more APs are required to transmit signal to it in order to meet the demand of DL's QoS.

Furthermore, we select one of the testing samples to study the convergence behavior of QT-SCA and to compare the performance of different methods. As shown in Fig. 7, it can be observed that our proposed QT-SCA method is able to converge quickly, within 6 iterations,

[12]Due to the unsatisfactory performance achieved by HGNN, FC-DNN and CNN as well as their poor scalability to the networks of varying sizes, in the rest of performance studies, we only consider the QT-SCA and greedy unfair methods, which provide the upper bound and lower bound performance, respectively, along with our CF-HGNN. The comparison with the HGNN, FC-DNN and CNN will not be further considered for the sake of brevity.

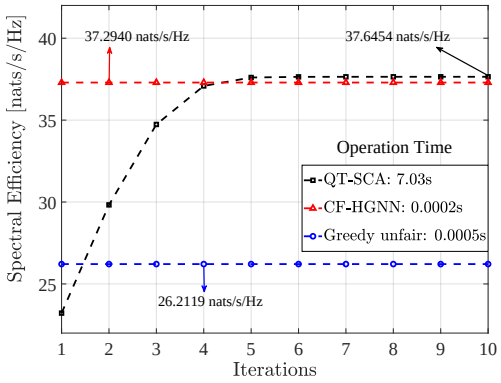

Fig. 7. Convergence behavior of QT-SCA and performance comparison among different methods when $L = 24$ and $D = 6$.

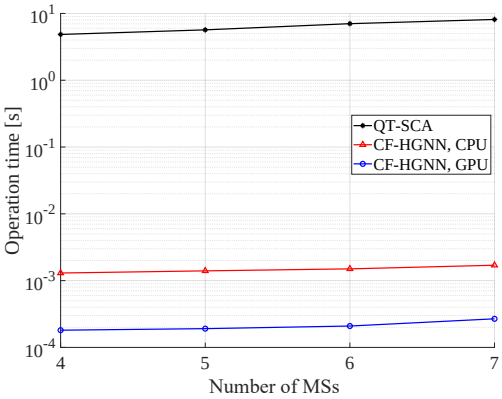

Fig. 8. Comparison of the operation time of QT-SCA and CF-HGNN.

and achieve the highest SE. Unfortunately, the QT-SCA is an online iterative optimization method, which has a high computational complexity and results in the largest operation time. By contrast, the CF-HGNN can be trained offline and the well-trained model can be directly applied to the testing samples. Hence, the CF-HGNN is capable of reaching 99% of the SE achieved by the QT-SCA, but only using 10^{-4} times of the operation time of the QT-SCA. As to the greedy unfair method, although it has a similar operation time as the CF-HGNN, its SE performance is significantly worse than that of the other two methods.

The comparison between QT-SCA and CF-HGNN in terms of computational complexity and operation time are then analyzed. According to [41], the approximated computational complexity of the QT-SCA method is $\mathcal{O}\big((LDM + 2DM + 3D\bar{M})^2(L + D + 3DM_{\text{sum}})^{2.5} + (L + D + 3DM_{\text{sum}})^{3.5}\big)$ per iteration. As to the CF-HGNN, the computational complexity is mainly due to the matrix computation, as shown in (10)-(13). Table III summarizes the results for the different values of L, D, M and $\bar{M}$, showing that when doubling the numbers of APs, MSs and subcarriers, the computational complexity of the QT-SCA increases much more quickly than that of the CF-HGNN, which is about three orders for the QT-SCA versus one order for the CF-HGNN. The operation time cost by the QT-SCA and CF-HGNN is plotted in Fig. 8. Explicitly, the CF-HGNN spends much less time than the QT-SCA to accomplish the PA. Moreover, thanks to the parallel computation of GPU, the CF-HGNN trained on GPU has the lowest operation time.

Next, we evaluate the generalization performance of the proposed CF-HGNN in MDD-CF networks with different cell sizes. As shown in Table IV (the SE of the CF-HGNN are normalized by that of the QT-SCA), the results under the Generalized CF-HGNN (GCF-HGNN) are obtained by the CF-HGNN model trained on the specific network with $S_{\text{D}} = 400$, while the results under the Dedicated CF-HGNN (DCF-HGNN) are obtained by the CF-HGNN models trained correspondingly using different cell sizes. It can be observed from the table that as the cell size reduces, the performance of the GCF-HGNN degrades slightly, but

TABLE III
COMPUTATIONAL COMPLEXITY COMPARISON

L	D	$M/\bar{M}$	Methods	
			QT-SCA	CF-HGNN
6	2	4/2	4.48×10^8	6.83×10^6
12	4	8/4	4.78×10^{11}	2.75×10^7
24	8	16/8	6.79×10^{14}	1.48×10^8

TABLE IV
GENERALIZATION TO DIFFERENT CELL SIZES.

S_{D}	QT-SCA (nats/s/Hz)	DCF-HGNN	GCF-HGNN
350	37.85	96.64%	95.19%
300	40.64	98.08%	93.13%
250	43.76	98.42%	91.84%
200	46.84	99.91%	91.78%
150	50.10	101.42%	92.79%

is still in the acceptable range. Note that, the DCF-HGNN finally outperforms the QT-SCA when $S_{\text{D}} = 150$, which means that the DCF-HGNN is capable of obtaining a better PA strategy in dense networks.

As the training of CF-HGNN is unsupervised and subject to four constraints as shown in (14), we next investigate the performance of CF-HGNN in terms of the constraint satisfaction. For this we should note that, although the problem of constraint violation is negligible in training samples, the well-trained model is used for implementing power allocation in the unknown testing samples. Hence, unlike the QT-SCA solving the problem online, there is no guarantee that all the constraints will be satisfied for every AP and MS in testing samples. To evaluate the level of constraint violation, we introduce two new performance metrics, namely the violation probability of constraint P_{V} and the mean violation error e_{V}. To elaborate on this point, we take power constraint of AP for example. As the total number of APs in the testing samples is 24000, if the number of APs violating the maximum power constraint P_l is N_{V}, then we have $P_{\text{V}} = \frac{N_{\text{V}}}{24000} \times 100\%$ and $e_{\text{V}} = \frac{\sum_{i=1}^{N_{\text{V}}}(P_i - P_l)}{24000}$. Hence, P_{V} can be used to reflect the ratios of APs/MSs in the testing samples violating the DL/UL QoS requirements or maximum power constraints, while e_{V} explains the extent of violation. The results are

TABLE V
CONSTRAINTS SATISFACTION

Parameters	Metrics		
$\kappa_1, \kappa_2, \kappa_3, \kappa_4$	SE	$P_{\rm V}$ for $(\chi_{\rm DL}, \chi_{\rm UL}, P_l, P_d)$	$e_{\rm V}$ for $(\chi_{\rm DL}, \chi_{\rm UL}, P_l, P_d)$
(0.1, 1, 0.1, 0.1)	34.40	(0%, 6.78%, 0.07%, 0%)	(0, 15×10^{-4}, 0.09×10^{-4}, 0)
(0.1, 5, 0.1, 0.1)	34.02	(0%, 4.67%, 0.06%, 0%)	(0, 3×10^{-4}, 0.1×10^{-4}, 0)
(0.1, 5, 1, 0.1)	33.45	(0%, 2.38%, 0%, 0.33%)	(0, 0.7×10^{-4}, 0, 1.3×10^{-4})

shown in Table V, from which we can know that the constraints on the APs/MSs transmit power and DL QoS can be easily satisfied in the testing samples with less than 1% violation probability. By contrast, since the single-antenna MSs have relatively small transmit power and the UL signal receiving at some APs may be severely influenced by the neighboring APs in close proximity, the QoS requirements of 6.78% of the UL MSs cannot be properly satisfied, whereas the violation error (i.e., $e_{\rm V} = 0.0015$) is minimal when compared with $\chi_{\rm UL} = 0.1$. Additionally, as shown in Table V, the $P_{\rm V}$ and $e_{\rm V}$ of $\chi_{\rm UL}$ can be significantly decreased by tuning the parameters κ_2 and κ_3, while the loss of spectral efficiency is limited and acceptable.

C. Scalability: Case 1

The simulation results in Section IV-B demonstrated that the CF-HGNN is able to achieve the similar performance as the QT-SCA. However, the CF-HGNN considered so far can only be applied to the specific MDD-CF networks with the fixed numbers of nodes and subcarriers, as the fully-connected liner layers in $\Xi_{\rm ada}$ and $\Xi_{\rm PA}$ act as identical matrices. With this regard, to enable the CF-HGNN to be adaptive to the varying MDD-CF networks, we now invoke the adaptive node embedding layer and adaptive output layer. In particular, we consider two cases regarding to the scalability of CF-HGNN. In Case 1, we assume a practical scenario where the considered area can only accommodate up to $L \leq L' = 24$ APs, and each AP is equipped with $N = 8$ antennas. We also assume that the number of MSs within this area is subject to $D \leq N$, and each AP is able to simultaneously serve all the MSs using, for example, ZF beamforming. Then, in order to allow the Adaptive CF-HGNN (ACF-HGNN) to be generalized for varying networks, 10000 MDD-CF network samples consisting of various numbers of nodes and subcarriers are used, where $L \in [8, 12, 16, 20, 24]$, $D \in [4, 5, 6, 7]$ and $M/\bar{M} \in [4/2, 16/8, 32/16]$[13]. For fair comparison, we also use 10000 MDD-CF network samples with the specific numbers of nodes and subcarriers to train the DCF-HGNN.

Table VI shows that by employing the adaptive layers, the ACF-HGNN can attain the relatively stable performance, when dealing with the various networks. Hence, it is feasible for implementing dynamic PA in MDD-CF networks. On the contrary, the QT-SCA and DCF-HGNN have to re-solve the complicated optimization problem or re-train the CF-HGNN, once the CF network has some changes in terms of the numbers of APs, MSs and subcarriers. Note that, in the table, the SE decreases with the increase of the number of subcarriers. This is because the total power allocated to subcarriers is constrained, while the SE is normalized by $M_{\rm sum}$, as shown in (7). Apparently, the total SE obtained by multiplying $M_{\rm sum}$ with the value in the table always increases with the increase of the number of subcarriers, which is attributed to the subcarrier diversity.

D. Scalability: Case 2

Although the proposed ACF-HGNN can handle the PA in various MDD-CF networks, it can hardly cut the mustard when the numbers of APs and MSs become too large, i.e., when $L \gg L'$ and $D \gg N$, as explained in Remark 3. Therefore, in Case 2, we resort to the user-centric clustering strategy to transform the dense graph into the sparse graph, thereby maintaining the scalability of the CF-HGNN for operation in the large-scale MDD-CF networks. For the sake of explanation, here we consider an extreme scenario, where each AP is only equipped with one antenna and serves only one MS using the ZF beamforming. Correspondingly, the clustering can be achieved in two steps[14]: 1) Initialize the set of APs serving MS d as $\mathcal{L}_d = \emptyset, \forall d = 1, ..., D$, and the set of MSs assigned to AP l as $\mathcal{D}_l = \emptyset, \forall l = 1, ..., L$. To guarantee a non-zero SE, each MS d is firstly assigned to a master AP by following the optimization of

$$l = \underset{l \in \{1,...,L\}, m \in \{1,...,M\}}{\operatorname{argmax}} \omega_{ldm}, \ \mathcal{L}_d = \{l\}, \ \mathcal{D}_l = \{d\} \ . \quad (16)$$

After this optimization, we have $|\mathcal{L}_d| = 1, \forall d = 1, ..., D$. 2) If there are still idle APs, which satisfy $\{l' | \mathcal{D}_{l'} = \emptyset\}$, allocate them to MSs according to the optimization of

$$d = \underset{d \in \{1,...,D\}, m \in \{1,...,M\}}{\operatorname{argmax}} \omega_{l'dm}, \ \mathcal{D}_{l'} = \{d\}, \ \mathcal{L}_d = \mathcal{L}_d \cup \{l'\} \ . \quad (17)$$

To train the Large-Scale ACF-HGNN (LSACF-HGNN), we have 10000 training samples collected from the networks with $L = 12$ single-antenna APs and $D = 6$ MSs uniformly distributed within an area of ($200\sqrt{2} \times$

[13]For the simplicity of training, the possible cases of nodes and subcarriers are limited. In practice, the size of training samples can be increased so as to include more combinations of nodes and subcarriers to enhance the scalability of ACF-HGNN.

[14]Note that the considered two-stage clustering approach is sub-optimal, and becomes less efficient in the case of $N > 1$, where each AP can simultaneously serve more than one MS using the increased spatial degrees of freedom. To this end, our future work motivates to propose a GNN-assisted deep Q-learning network so as to obtain the optimal user grouping and PA at the same time.

TABLE VI
GENERALIZATION TO THE DIFFERENT NUMBERS OF APS, MSS AND SUBCARRIERS.

L	D	$M/\bar{M}$	QT-SCA (nats/s/Hz)	DCF-HGNN	ACF-HGNN	Greedy unfair
24	4	4/2	26.42	98.07%	94.14%	74.45%
	5		31.34	98.02%	94.51%	74.06%
	6		34.23	97.78%	94.77%	73.06%
	7		36.24	98.18%	95.45%	73.68%
20	6	4/2	33.04	98.09%	97.22%	72.79%
16			29.99	97.70%	95.07%	71.16%
12			25.69	98.52%	94.08%	69.95%
8			21.13	97.40%	94.46%	68.67%
16	6	32/16	9.26	98.81%	91.58%	72.35%
		16/8	15.53	99.03%	91.50%	68.45%

TABLE VII
GENERALIZATION TO THE LARGE-SCALE MDD-CF NETWORKS.

S_{D}	L	D	QT-SCA (nats/s/Hz)	LSACF-HGNN	Greedy unfair
400	24	12	22.93	93.68%	65.68%
450	30	15	28.28	92.33%	65.38%
500	38	19	35.18	91.42%	65.66%
$400\sqrt{2}$	48	24	43.93	88.05%	65.65%
$400\sqrt{3}$	72	36	63.92	82.09%	65.35%
800	96	48	82.10	80.58%	67.23%

$200\sqrt{2})\mathrm{m}^2$. We then increase the number of APs and MSs in testing samples while the densities of AP and MSs are fixed. Note that all the involved training and testing samples have been pre-processed by the proposed clustering algorithm.

As shown in Table VII, when $400 \leq S_D \leq 500$, the LSACF-HGNN exhibits a good scalability and its performance loss is no more than 9% when compared with QT-SCA. Moreover, when S_D is further enlarged from $400\sqrt{2}$m to 800m, the performance loss is around 20%. The reason behind this undesirable performance loss in very large networks can be explained as follows. Although the densities of APs and MSs are kept unchanged as S_D becomes wider, the total numbers of APs and MSs are significantly increased. In this case, it is expected that some small sub-areas may have extremely dense APs and/or MSs. Consequently, each AP and MS having only one communication path may experience lots of interference paths during message passing, resulting in that the model is hard to extract useful information. In other words, the LSACF-HGNN may require extra training or an improved model structure to manage the CLI for such high-density sub-areas, which is however out of the scope of this paper but left for our future research.

Nevertheless, we should mention that, despite the undesirable performance of the LSACF-HGNN in very large areas, it is still a highly promising method, significantly outperforming the greedy unfair PA. Furthermore, as seen in Table III, the computational complexity of the conventional non-convex optimization methods, e.g., QT-SCA, increases sharply as the size of networks becomes larger, and hence cannot efficiently handle the PA in large-scale networks. On the other side, as the PA methods empowered by DNN-, CNN- or DRL-based models have no comparable scalability with CF-HGNN [9, 10, 12], their model training relying on large-scale networks impose heavy burden on system's computational resources. By contrast, considering the fact that all the results of LSACF-HGNN in Table VII are obtained using the model, which is trained only on the small-scale network samples, the performance of LSACF-HGNN is still quite competitive.

V. CONCLUSIONS

In this paper, we proposed a distributed MDD-CF system, and investigated the PA at both AP and MS sides for SE maximization under the constraints of QoS requirements. In order to solve the non-convex and NP-hard PA problem, we first proposed the QT-SCA algorithm, which achieves the optimization in the classic way. Then, the CF-HGNN was proposed to solve the optimization from a learning perspective. Our studies and numerical results show that the CF-HGNN is capable of achieving the SE performance comparable to the QT-SCA but demanding much less operation time and computational complexity. The CF-HGNN significantly outperforms the greedy unfair method in terms of SE performance. Furthermore, with the aid of adaptive node embedding layer and adaptive output layer, the CF-HGNN can implement PA in the MDD-CF networks with various numbers of APs, MSs and subcarriers. Additionally, with the aid of user clustering, the CF-HGNN trained based on a relatively small-scale MDD-CF network can be generalized for operation in the large-scale MDD-CF networks.

APPENDIX A
QT-SCA OPTIMIZATION

As the main function of (7) belongs to the general multiple-ratio concave-convex fractional programming

problem, it can be firstly reformulated by the QT method [42] as

$$\max_{\boldsymbol{p},\boldsymbol{z}} \frac{1}{M_{\text{sum}}} \sum_{d=1}^{D} \Bigg(\sum_{m=1}^{M} \ln\left(1+2z_{dm}\sqrt{A_{d,m}(\boldsymbol{p})} - z_{dm}^2 B_{d,m}(\boldsymbol{p})\right) + \sum_{\bar{m}=1}^{\bar{M}} \ln(1+2z_{d\bar{m}}\sqrt{A_{d,\bar{m}}(\boldsymbol{p})} - z_{d\bar{m}}^2 B_{d,\bar{m}}(\boldsymbol{p})\Bigg), \tag{18}$$

where $\text{SINR}_{d,m} = \frac{A_{d,m}(\boldsymbol{p})}{B_{d,m}(\boldsymbol{p})}$, $\text{SINR}_{d,\bar{m}} = \frac{A_{d,\bar{m}}(\boldsymbol{p})}{B_{d,\bar{m}}(\boldsymbol{p})}$, $\boldsymbol{p} = (\{p_{ldm}\},\{p_{d\bar{m}}\})$. In (18), $\ln(1+x)$ is a non-decreasing and concave function. For a given $\boldsymbol{p}$, both $\text{SINR}_{d,m}$ and $\text{SINR}_{d,\bar{m}}$ are also concave-convex. Hence, when $\boldsymbol{p}$ is fixed, the optimal $\boldsymbol{z} = (\{z_{dm}\},\{z_{d\bar{m}}\})$ maximizing (18) can be obtained as $\boldsymbol{z}^* = \frac{\sqrt{A(\boldsymbol{p})}}{B(\boldsymbol{p})}$. Then, given a fixed value of $\boldsymbol{z}$, the problem (18) is a concave maximization problem over $\boldsymbol{p}$.

However, the constraints of (7d) and (7e) are still nonconvex, which need to be approximated by the convex ones using the SCA method. As shown in (7d) and (7e), these original constraints are extremely complicated, which contain the sum of M and $\bar{M}$ nonconvex components, respectively. Hence, we firstly simplify them to the following ones:

$$\text{SINR}_{d,m} \geq e^{\frac{\chi_{\text{DL}}}{M}} - 1, \ \forall d \in \mathcal{D}, m \in \mathcal{M}, \tag{19}$$

$$\text{SINR}_{d,\bar{m}} \geq e^{\frac{\chi_{\text{UL}}}{M}} - 1, \ \forall d \in \mathcal{D}, \bar{m} \in \bar{\mathcal{M}}. \tag{20}$$

Then, based on (6), the simplified constraint (19) can be equivalently written as

$$\begin{cases} \text{SINR}_{d,m} \triangleq \varpi_{d,m}^2/\psi_{d,m} \geq e^{\frac{\chi_{\text{DL}}}{M}} - 1, & \text{(21a)} \\ 0 < \varpi_{d,m} \leq \sum_{l\in\mathcal{L}} \sqrt{p_{ldm}}\omega_{ldm}, & \text{(21b)} \\ \psi_{d,m} \geq \xi_d^{\text{SI}}\Theta_{\text{DL}} + \sigma^2, & \text{(21c)} \end{cases}$$

where $\varpi_{d,m}$ and $\psi_{d,m}$ are new variables, while (21b) and (21c) are linear constraints. For (21a), since the function $f_{\text{ca}}(\varpi_{d,m},\psi_{d,m}) \triangleq \varpi_{d,m}^2/\psi_{d,m}$ with $(\varpi_{d,m},\psi_{d,m}) \in \mathbb{R}_{++}^2$ is convex, it can be approximated with the aid of the SCA properties as [43]

$$\begin{aligned} f_{\text{ca}}(\varpi_{d,m},\psi_{d,m}) &\geq \frac{2\varpi_{d,m}^{(t)}}{\psi_{d,m}^{(t)}}\varpi_{d,m} - \frac{(\varpi_{d,m}^{(t)})^2}{(\psi_{d,m}^{(t)})^2}\psi_{d,m} \\ &:= f_{\text{ca}}^{(t)}(\varpi_{d,m},\psi_{d,m}), \end{aligned} \tag{22}$$

where $(\varpi_{d,m}^{(t)},\psi_{d,m}^{(t)})$ is the feasible point obtained at the t-th iteration. Consequently, (21a) can be substituted by the new constraint given by

$$f_{\text{ca}}^{(t)}(\varpi_{d,m},\psi_{d,m}) \geq e^{\frac{\chi_{\text{DL}}}{M}} - 1. \tag{23}$$

Following the same spirit, (20) can be equivalently expressed by the following convex constraints:

$$\begin{cases} f_{\text{ca}}^{(t)}(\sqrt{\varpi_{d,\bar{m}}},\psi_{d,\bar{m}}) \geq e^{\frac{\chi_{\text{UL}}}{M}} - 1, & \text{(24a)} \\ 0 < \varpi_{d,\bar{m}} \leq p_{d\bar{m}}L^2, & \text{(24b)} \\ \psi_{d,m} \geq \sum_{l\in\mathcal{L}} \upsilon_{ldm}\left(\xi_l^{\text{SI}}\Theta_{\text{UL}} + \sigma^2\right). & \text{(24c)} \end{cases}$$

To this point, the optimization problem (7) can be rewritten as

$$\begin{aligned} \max_{\boldsymbol{p},\boldsymbol{z},\boldsymbol{\varpi},\boldsymbol{\psi}} & \frac{1}{M_{\text{sum}}} \sum_{d=1}^{D} \Bigg(\sum_{m=1}^{M} \ln\left(1+2z_{dm}\sqrt{A_{d,m}(\boldsymbol{p})} - z_{dm}^2 B_{d,m}(\boldsymbol{p})\right) \\ & + \sum_{\bar{m}=1}^{\bar{M}} \ln(1+2z_{d\bar{m}}\sqrt{A_{d,\bar{m}}(\boldsymbol{p})} - z_{d\bar{m}}^2 B_{d,\bar{m}}(\boldsymbol{p})\Bigg) \\ \text{s.t.} \ & z_{dm} \in \mathbb{R}, \ \forall d \in \mathcal{D}, m \in \mathcal{M}, \ z_{d\bar{m}} \in \mathbb{R}, \ \forall d \in \mathcal{D}, \bar{m} \in \bar{\mathcal{M}}, \\ & \text{(7b)}, \text{(7c)}, \text{(21b)}, \text{(21c)}, \text{(23)}, \text{(24)}. \end{aligned} \tag{25}$$

During the optimization of (25), $\boldsymbol{p}$ and $\boldsymbol{z}$ are iteratively optimized. Hence, the initialization of $\boldsymbol{p},\boldsymbol{\varpi},\boldsymbol{\psi}$ is of paramount importance, which can be obtained by solving the optimization problem

$$\begin{aligned} \underset{\boldsymbol{p},\boldsymbol{\varpi},\boldsymbol{\psi}}{\text{argmax}} & \sum_{d=1}^{D} \left(\sum_{m=1}^{M} \alpha_{d,m} + \sum_{\bar{m}=1}^{\bar{M}} \alpha_{d,\bar{m}} \right) \\ \text{s.t.} \ & \alpha_{d,m} \leq 0, \alpha_{d,\bar{m}} \leq 0, \forall d \in \mathcal{D}, m \in \mathcal{M}, \bar{m} \in \bar{\mathcal{M}}, \\ & 2\varpi_{d,m} - \psi_{d,m} \geq e^{\frac{\chi_{\text{DL}}}{M}} - 1 + \alpha_{d,m}, \forall d \in \mathcal{D}, m \in \mathcal{M}, \\ & 2\varpi_{d,\bar{m}} - \psi_{d,\bar{m}} \geq e^{\frac{\chi_{\text{UL}}}{M}} - 1 + \alpha_{d,\bar{m}}, \forall d \in \mathcal{D}, \bar{m} \in \bar{\mathcal{M}}, \\ & \text{(7b)}, \text{(7c)}, \text{(21b)}, \text{(21c)}, \text{(24b)}, \text{(24c)}, \end{aligned} \tag{26}$$

where $(\{\alpha_{d,m}\},\{\alpha_{d,\bar{m}}\})$ are new variables. When the objective function of (26) is close to zero, the initial $\boldsymbol{p},\boldsymbol{\varpi},\boldsymbol{\psi}$ can be appropriately obtained.

The overall QT-SCA algorithm is summarized as Algorithm 1. Note that, the proposed QT-SCA algorithm relies mainly on the QT and SCA methods, the detailed proof of their convergence can be found in [42] and [43], respectively. Additionally, the convergence behavior and computational complexity of the algorithm are evaluated in Section IV-B.

Algorithm 1: QT-SCA Algorithm for SE maximization in MDD-CF

Initialization:
Compute $\{\omega_{ldm}\},\{\upsilon_{ld\bar{m}}\},\forall l,d,m,\bar{m}$;
Set $t=0$ and compute $\boldsymbol{p}^{(t)},\boldsymbol{\varpi}^{(t)},\boldsymbol{\psi}^{(t)}$ by solving optimization problem (26);
[QT Iteration]
  repeat
    Compute $\boldsymbol{z}^{(t)}$ using $\boldsymbol{z}^{(t)} = \frac{\sqrt{A(\boldsymbol{p}^{(t)})}}{B(\boldsymbol{p}^{(t)})}$ for a fixed $\boldsymbol{p}^{(t)}$;
    Update $\boldsymbol{p}^{(t+1)}$ via (25), for a fixed $\boldsymbol{z}^{(t)}$; Update $\varpi_{d,m}^{(t+1)},\varpi_{d,\bar{m}}^{(t+1)},\psi_{d,m}^{(t+1)},\psi_{d,\bar{m}}^{(t+1)}$;
    Set $t=t+1$;
  until Convergence;
end
Output: $\boldsymbol{p}$

References

[1] Ö. T. Demir, E. Björnson, L. Sanguinetti *et al.*, "Foundations of user-centric cell-free massive mimo," *Foundations and Trends® in Signal Proc.*, vol. 14, no. 3-4, pp. 162–472, 2021.

[2] S. Goyal, P. Liu, S. S. Panwar, R. A. Difazio, R. Yang, and E. Bala, "Full duplex cellular systems: will doubling interference prevent doubling capacity?" *IEEE Com. Mag.*, vol. 53, no. 5, pp. 121–127, 2015.

[3] H. V. Nguyen, et.al, "On the spectral and energy efficiencies of full-duplex cell-free massive MIMO," *IEEE J. on Selected Areas in Com.*, vol. 38, no. 8, pp. 1698–1718, 2020.

[4] B. Li, L.-L. Yang, R. Maunder, S. Sun, and P. Xiao, "Spectral-efficiency of cell-free massive MIMO with multicarrier-division duplex," *arXiv preprint arXiv:2206.08774*, 2022.

[5] B. Li, L.-L. Yang, R. G. Maunder, P. Xiao, and S. Sun, "Multicarrier-division duplex: A duplexing technique for the shift to 6G wireless communications," *IEEE Veh. Tech. Mag.*, 2021.

[6] S. Chakraborty, Ö. T. Demir, E. Björnson, and P. Giselsson, "Efficient downlink power allocation algorithms for cell-free massive mimo systems," *IEEE Open J. of the Com. Society*, vol. 2, pp. 168–186, 2020.

[7] F. Fang, Z. Ding, W. Liang, and H. Zhang, "Optimal energy efficient power allocation with user fairness for uplink MC-NOMA systems," *IEEE Wireless Com. Letters*, vol. 8, no. 4, pp. 1133–1136, 2019.

[8] J.-W. Li and C. Lin, "On the optimal power allocation for two-way full-duplex af relay networks," *IEEE Trans. on Signal Proc.*, vol. 65, no. 21, pp. 5702–5715, 2017.

[9] W. Lee, M. Kim, and D.-H. Cho, "Deep power control: Transmit power control scheme based on convolutional neural network," *IEEE Com. Letters*, vol. 22, no. 6, pp. 1276–1279, 2018.

[10] L. Luo, et.al, "Downlink power control for cell-free massive MIMO with deep reinforcement learning," *IEEE Trans. on Veh. Tech.*, 2022.

[11] M. Bashar, et.al, "Deep learning-aided finite-capacity fronthaul cell-free massive mimo with zero forcing," in *ICC'20*. IEEE, 2020, pp. 1–6.

[12] M. Zaher, Ö. T. Demir, E. Björnson, and M. Petrova, "Learning-based downlink power allocation in cell-free massive MIMO systems," *arXiv preprint arXiv:2109.03128*, 2021.

[13] Y. Shen, et.al, "Graph neural networks for scalable radio resource management: Architecture design and theoretical analysis," *IEEE J. on Selected Areas in Com.*, vol. 39, no. 1, pp. 101–115, 2020.

[14] A. Chowdhury, G. Verma, C. Rao, A. Swami, and S. Segarra, "Unfolding WMMSE using graph neural networks for efficient power allocation," *IEEE Trans. on Wireless Com.*, vol. 20, no. 9, pp. 6004–6017, 2021.

[15] M. Eisen and A. Ribeiro, "Optimal wireless resource allocation with random edge graph neural networks," *IEEE Trans. on Signal Proc.*, vol. 68, pp. 2977–2991, 2020.

[16] C. Zhang, et.al, "Heterogeneous graph neural network," in *Proc. of the 25th ACM SIGKDD*, 2019, pp. 793–803.

[17] X. Zhang, et.al, "Scalable power control/beamforming in heterogeneous wireless networks with graph neural networks," in *2021 IEEE GLOBECOM'21*. IEEE, 2021, pp. 01–06.

[18] T. Jiang, H. V. Cheng, and W. Yu, "Learning to reflect and to beamform for intelligent reflecting surface with implicit channel estimation," *IEEE J. on Selected Areas in Comm.*, vol. 39, no. 7, pp. 1931–1945, 2021.

[19] J. Kim, H. Lee, S.-E. Hong, and S.-H. Park, "A bipartite graph neural network approach for scalable beamforming optimization," *IEEE Trans. on Wireless Com.*, 2022.

[20] J. Guo and C. Yang, "Learning power allocation for multi-cell-multi-user systems with heterogeneous graph neural networks," *IEEE Trans. on Wireless Com.*, vol. 21, no. 2, pp. 884–897, 2021.

[21] B. Li, et.al, "Self-interference cancellation and channel estimation in multicarrier-division duplex systems with hybrid beamforming," *IEEE Access*, vol. 8, pp. 160 653–160 669, 2020.

[22] B. Li, et.al, "Resource allocation in millimeter-wave multicarrier-division duplex systems with hybrid beamforming," *IEEE Trans. on Veh. Tech.*, vol. 70, no. 8, pp. 7921–7935, 2021.

[23] B. P. Day, et.al, "Full-duplex MIMO relaying: Achievable rates under limited dynamic range," *IEEE J. on Selected Areas in Com.*, vol. 30, no. 8, pp. 1541–1553, 2012.

[24] X. Xia, et.al, "Joint user selection and transceiver design for cell-free with network-assisted full duplexing," *IEEE Trans. on Wireless Com.*, 2021.

[25] D. W. K. Ng, et.al, "Power efficient resource allocation for full-duplex radio distributed antenna networks," *IEEE Trans. on Wireless Com.*, vol. 15, no. 4, pp. 2896–2911, 2012.

[26] A. Chowdhury, et.al, "Can dynamic TDD enabled half-duplex cell-free massive MIMO outperform full-duplex cellular massive MIMO?" *IEEE Trans. on Com.*, vol. 70, no. 7, pp. 4867–4883, 2022.

[27] E. Björnson, J. Hoydis, L. Sanguinetti *et al.*, "Massive MIMO networks: Spectral, energy, and hardware efficiency," *Foundations and Trends® in Signal Proc.*, vol. 11, no. 3-4, pp. 154–655, 2017.

[28] Y. Jiang, et.al, "Performance analysis of ZF and MMSE equalizers for MIMO systems: An in-depth study of the high SNR regime," *IEEE Trans. on Inf. Theory*, vol. 57, no. 4, pp. 2008–2026, 2011.

[29] Y. Sun and J. Han, "Mining heterogeneous information networks: a structural analysis approach," *ACM SIGKDD Explorations Newsletter*, vol. 14, no. 2, pp. 20–28, 2013.

[30] X. Wang, H. Ji, C. Shi, B. Wang, Y. Ye, P. Cui, and P. S. Yu, "Heterogeneous graph attention network," in *The world wide web conference*, 2019, pp. 2022–2032.

[31] W. Cui, K. Shen, and W. Yu, "Spatial deep learning for wireless scheduling," *IEEE J. on Selected Areas in Com.*, vol. 37, no. 6, pp. 1248–1261, 2019.

[32] S. Buzzi and C. D'Andrea, "Cell-free massive MIMO: User-centric approach," *IEEE Wireless Com. Letters*, vol. 6, no. 6, pp. 706–709, 2017.

[33] P. Veličković, G. Cucurull, A. Casanova, A. Romero, P. Lio, and Y. Bengio, "Graph attention networks," *arXiv:1710.10903*, 2017.

[34] D. P. Kingma and J. Ba, "Adam: A method for stochastic optimization," *arXiv:1412.6980*, 2014.

[35] K. E. Kolodziej, B. T. Perry, and J. S. Herd, "In-band full-duplex technology: Techniques and systems survey," *IEEE Trans. on Micro. Theory and Tech.*, vol. 67, no. 7, pp. 3025–3041, 2019.

[36] M. Fey and J. E. Lenssen, "Fast graph representation learning with pytorch geometric," *arXiv:1903.02428*, 2019.

[37] S. Patro and K. K. Sahu, "Normalization: A preprocessing stage," *arXiv preprint arXiv:1503.06462*, 2015.

[38] M. Grant and S. Boyd, "CVX: Matlab software for disciplined convex programming, version 2.1," http://cvxr.com/cvx, Mar. 2014.

[39] J. Jang and K. B. Lee, "Transmit power adaptation for multiuser OFDM systems," *IEEE J. on Selected Areas in Com.*, vol. 21, no. 2, pp. 171–178, 2003.

[40] M. Labana and W. Hamouda, "Unsupervised deep learning approach for near optimal power allocation in cran," *IEEE Trans. on Veh. Tech.*, vol. 70, no. 7, pp. 7059–7070, 2021.

[41] D. Peaucelle, et.al, "User's guide for SEDUMI interface 1.04," *LAAS-CNRS, Toulouse*, 2002.

[42] K. Shen and W. Yu, "Fractional programming for communication systems-part I: Power control and beamforming," *IEEE Trans. on Signal Proc.*, vol. 66, no. 10, pp. 2616–2630, 2018.

[43] B. R. Marks and G. P. Wright, "A general inner approximation algorithm for nonconvex mathematical programs," *Operations Research*, vol. 26, no. 4, pp. 681–683, 1978.

Bohan-Li received his MEng degree from Beijing University of Posts and Telecommunications in 2018, and his PhD degree from the University of Southampton in 2022. Currently, he works as a research fellow at the University of Leicester, UK. In recent years, his research has been mainly focused on the multicarrier-division duplex based wireless communications . He also has research interest in various techniques for the future generations of wireless systems, including full duplex communications, smart wireless transceivers, mmWave massive MIMO, cell-free massive MIMO, deep reinforcement learning and graph neural networks for optimization of wireless systems.

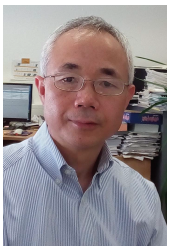

Lie-Liang Yang (Fellow, IEEE) is the professor of Wireless Communications in the School of Electronics and Computer Science at the University of Southampton, UK. He received his MEng and PhD degrees in communications and electronics from Northern (Beijing) Jiaotong University, Beijing, China in 1991 and 1997, respectively, and his BEng degree in communications engineering from Shanghai TieDao University, Shanghai, China in 1988. He has research interest in wireless communications, wireless networks and signal processing for wireless communications, as well as molecular communications and nano-networks. He has published 400+ research papers in journals and conference proceedings, authored/co-authored three books and also published several book chapters. The details about his research publications can be found at https://www.ecs.soton.ac.uk/people/llyang. He is a fellow of both the IEEE and the IET, and was a distinguished lecturer of the IEEE VTS. He served as an associate editor to various journals, and is currently a senior editor to the IEEE Access and a subject editor to the Electronics Letters. He also acted different roles for organization of conferences.

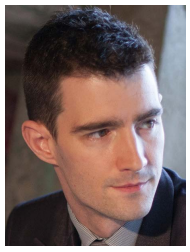

Robert G. Maunder (Senior Member, IEEE) has been studying with the School of Electronics and Computer Science, University of Southampton, Southampton, UK, since October 2000. He received the B.Eng. (first class hons.) degree in electronic engineering in July 2003 and the Ph.D. degree in telecommunications in December 2007. In November 2007, he began a lectureship, in March 2013, was promoted to an Associate Professor, and in August 2017, to a Professor. He has authored or coauthored a number of IEEE papers in his areas or research, which include joint source/channel coding and the holistic design of algorithms and hardware implementations for wireless communications. He was awarded Chartered Engineer status of the IET in November 2013 and Fellow status of the IET in January 2017. He is the Founder and CTO of AccelerComm Ltd, Southampton, U.K., which is commercializing his research as soft-IP.

Songlin Sun (Senior Member, IEEE) is a professor in the School of Information and Communication Engineering, Beijing University of Posts and Telecommunications, Beijing, China. He received his M.S. degree in signal and information processing from Shandong University of Technology in January 2000 and his Ph.D. degree in communication and information systems from the Beijing University of Posts and Telecommunications in 2003. His research interests include signal processing in wireless communication, video code, and multimedia transmission.

Pei Xiao (Senior Member, IEEE) is a professor of Wireless Communications at the Institute for Communication Systems (ICS), home of 5GIC and 6GIC at the University of Surrey. He received the PhD degree from Chalmers University of Technology, Gothenburg, Sweden in 2004. He is currently the technical manager of 5GIC/6GIC, leading the research team in the new physical layer work area, and coordinating/supervising research activities across all the work areas (https://www.surrey.ac.uk/institute-communication-systems/5g-6g-innovation-centre). Prior to this, he worked at Newcastle University and Queen?s University Belfast. He also held positions at Nokia Networks in Finland. He has published extensively in the fields of communication theory, RF and antenna design, signal processing for wireless communications, and is an inventor on over 15 recent 5GIC patents addressing bottleneck problems in 5G systems.